JOURNAL OF PETROLOGY | VOLUME 52 | NUMBERS 7 & 8 | PAGES 1243–1263 | 2011 | doi:10.1093/petrology/egq089

Fe–Mg Partitioning between Olivine and High-magnesian Melts and the Nature of Hawaiian Parental Liquids

ANDREW K. MATZEN*, MICHAEL B. BAKER, JOHN R. BECKETT AND EDWARD M. STOLPER

DIVISION OF GEOLOGICAL AND PLANETARY SCIENCES 170-25, CALTECH, PASADENA, CA 91125, USA

RECEIVED JANUARY 21, 2010; ACCEPTED NOVEMBER 30, 2010
ADVANCE ACCESS PUBLICATION JANUARY 18, 2011

We conducted 1 atm experiments on a synthetic Hawaiian picrite at fO_2 values ranging from the quartz–fayalite–magnetite (QFM) buffer to air and temperatures ranging from 1302 to 1600°C. Along the QFM buffer, olivine is the liquidus phase at ~1540°C and small amounts of spinel (<0·2 wt %) are present in experiments conducted at and below 1350°C. The olivine becomes progressively more ferrous with decreasing temperature [$Fo_{92·3}$ to $Fo_{87·3}$, where $Fo = 100 \times Mg/(Mg + Fe)$, atomic]; compositions of coexisting liquids reflect the mode and composition of the olivine with concentrations of SiO_2, TiO_2, Al_2O_3, and CaO increasing monotonically with decreasing temperature, those of NiO and MgO decreasing, and FeO (all Fe as FeO) remaining roughly constant. An empirical relationship based on our data, $T(°C) = 19·2 \times (MgO$ in liquid, wt %$) + 1048$, provides a semi-quantitative geothermometer applicable to a range of Hawaiian magma compositions. The olivine–liquid exchange coefficient, $K_{D,Fe^{2+}-Mg} = (FeO/MgO)^{ol}/(FeO/MgO)^{liq}$, is 0·345 ± 0·009 (1σ) for our 11 experiments. A literature database of 446 1 atm experiments conducted within 0·25 log units of the QFM buffer (QFM ± 0·25) yields a median $K_{D,Fe^{2+}-Mg}$ of 0·34; $K_{D,Fe^{2+}-Mg}$ values from single experiments range from 0·41 to 0·13 and are correlated with SiO_2 and alkalis in the liquid, as well as the forsterite (Fo) content of the olivine. For 78 experiments with broadly tholeiitic liquid compositions (46–52 wt % SiO_2 and ≤ 3 wt % $Na_2O + K_2O$) coexisting with $Fo_{92–80}$ olivines, and run near QFM (QFM ± 0·25), $K_{D,Fe^{2+}-Mg}$ is approximately independent of composition with a median value of 0·340 ± 0·012 (error is the mean absolute deviation of the 78 olivine–glass pairs from the database that meet these compositional criteria), a value close to the mean value of 0·343 ± 0·008 from our QFM experiments. Thus, over the composition range encompassed by Hawaiian tholeiitic lavas and their parental melts, $K_{D,Fe^{2+}-Mg} \sim 0·34$ and, given the redox conditions and a Fo content for the most magnesian olivine phenocrysts, a parental melt composition can be reconstructed. The calculated compositions of the parental melts are sensitive to the input parameters, decreasing by ~1 wt % MgO for every log unit increase in the selected fO_2, every 0·5 decrease in the Fo-number of the target olivine, and every 0·015 decrease in $K_{D,Fe^{2+}-Mg}$. For plausible ranges in redox conditions and Fo-number of the most MgO-rich olivine phenocrysts, the parental liquids for Hawaiian tholeiites are highly magnesian, in the range of 19–21 wt % MgO for Kilauea, Mauna Loa and Mauna Kea.*

KEY WORDS: *Hawaii; parental liquids; Fe–Mg partitioning; olivine*

INTRODUCTION

Knowledge of the partitioning of elements between coexisting solid and liquid phases is critical for deciphering and modeling igneous processes. Hardly a paper is written on igneous petrogenesis today without referring to solid–liquid partition coefficients: examples include the modeling of evolving liquid compositions generated during partial melting and the liquid lines of descent of cooling magmas (e.g. Grove *et al.*, 1992; Nielsen & DeLong, 1992; Herzberg & O'Hara, 2002), reconstruction of the compositions of parental or primary liquids from the compositions of fractionated magmas (e.g. Baker *et al.*, 1996; Putirka *et al.*, 2007), and modeling the evolution of liquid compositions on the basis of cumulus phases (e.g. Longhi, 1982; Bédard, 1994; Thy *et al.*, 2006). The partitioning of major and minor elements between olivine and liquid is of particular

*Corresponding author. E-mail: amatzen@caltech.edu

importance because olivine is a ubiquitous phase in a broad range of mafic and ultramafic igneous rocks in the upper mantle, and the fractionation or accumulation of this phase exerts a major control on observed variations in magma composition (e.g. for Hawaii: Powers, 1955; Macdonald & Katsura, 1964; Clague *et al.*, 1991). It is, therefore, not surprising that there has been considerable experimental work over several decades aimed at quantifying the partitioning of major and minor elements between olivine and liquid in relevant igneous systems (e.g. Roeder & Emslie, 1970; Hart & Davis, 1978; Beattie *et al.*, 1991; Mallmann & O'Neill, 2009) and complementary development of empirical and thermodynamic models of the experimental data (e.g. Longhi *et al.*, 1978; Ford *et al.*, 1983; Hirschmann & Ghiorso, 1994; Toplis, 2005). Partitioning of Fe^{2+} and Mg between olivine and liquid is a natural starting point for such studies given that these are the dominant exchangeable cations in olivine from the Earth and other planets. Roeder & Emslie (1970) were the first to pair these elements in an exchange reaction between olivine and melt for use in correlating data in both experimental and natural systems. Based on 1 atm experiments on three Hawaiian basalts, they showed that the olivine (ol)–liquid (liq) exchange coefficient, $K_{D,Fe^{2+}-Mg} = (FeO/MgO)^{ol}/(FeO/MgO)^{liq}$, where FeO and MgO refer to concentrations (by weight), is $0{\cdot}30 \pm 0{\cdot}03$ and, within the resolution of their data, is independent of temperature and liquid composition. Later work considerably expanded the range of pressure, temperature, and liquid composition and showed that liquid composition does in fact exert a significant effect on $K_{D,Fe^{2+}-Mg}$ (e.g. Sack *et al.*, 1987; Gee & Sack, 1988). There have been numerous attempts to formulate expressions for $K_{D,Fe^{2+}-Mg}$ as a function of these variables (e.g. Longhi *et al.*, 1978; Ford *et al.*, 1983; Gee & Sack, 1988; Snyder & Carmichael, 1992; Sobolev & Nikogosian, 1994; Herzberg & O'Hara, 2002; Toplis, 2005) and various constant values of $K_{D,Fe^{2+}-Mg}$ have been proposed for specific applications (e.g. Nisbet *et al.*, 1987; Putirka *et al.*, 2007). Nevertheless, the Roeder & Emslie value of 0·30 is still a convenient reference point commonly used in petrological modeling (e.g. Garcia, 1996; Rhodes & Vollinger, 2004).

The paucity of experiments on highly magnesian liquids with compositions similar to those of naturally occurring magmas is problematic because estimates of parental or primary liquid compositions for Hawaii and other localities (e.g. Gorgona komatiites and picrites from Baffin Island, western Greenland, and Ontong–Java Plateau: Clague et al., 1991; Baker et al., 1996; Herzberg & O'Hara, 2002; Stolper et al., 2004; Herzberg et al., 2007) and liquids produced in high-pressure melting experiments on ultramafic compositions (e.g. Kushiro & Walter, 1998; Walter, 1998) often have more than 16 wt % MgO. Although a large number of olivine–liquid pairs are available in the literature (we have a compilation containing 1179 pairs), we are aware of only 24 with glass compositions similar to naturally occurring liquids (non-zero concentrations of TiO_2, Al_2O_3, FeO, MgO, CaO, and Na_2O) with ≥16 wt % MgO and for none of these high-MgO liquids was Fe^{3+}/Fe^{2+} actually measured. Thus, the effects of high MgO and the Fe^{3+}/Fe^{2+} ratio on Fe–Mg partitioning between olivine and liquid are poorly known, yet they are important for petrologic modeling. A major motivation for the study reported here is to extend the dataset on $K_{D,Fe^{2+}-Mg}$ to include experiments on magmatic liquids with high MgO contents conducted under well-characterized and controlled redox conditions.

In this study, we present the results of 1 atm experiments on a synthetic analog of a Hawaiian picrite (25·7 wt % MgO, 45·7 wt % SiO_2). Most of the experiments were performed near the quartz–fayalite–magnetite buffer (QFM), but two experiments were conducted under more oxidizing conditions [nickel–nickel oxide buffer (NNO) and air] to explore the effect of varying Fe^{3+}/Fe^{2+} in the liquid on $K_{D,Fe^{2+}-Mg}$. Glasses from two of the experiments (air and QFM) were also analyzed for FeO by wet chemistry, thereby allowing the determination of $K_{D,Fe^{2+}-Mg}$ independent of any Fe^{3+}/Fe^{2+} algorithm. In addition, we compiled a set of 1 atm olivine–liquid pairs from the literature encompassing fO_2 values ranging from slightly below the iron–wüstite (IW) buffer to air and MgO concentrations in the liquid from 1·3 to 28·6 wt %. Finally, we used this database together with the results of our experiments to constrain $K_{D,Fe^{2+}-Mg}$ for highly magnesian liquids and to reconstruct parental Hawaiian magma compositions.

EXPERIMENTAL AND ANALYTICAL TECHNIQUES

Starting composition

The starting composition for this study, Syn-HP1 (Table 1), is based on whole-rock analyses of 'low-SiO_2' Mauna Kea basalts from the Hawaii Scientific Drilling Project (HSDP) (Rhodes & Vollinger, 2004). We chose the 'low-SiO_2' array (Stolper *et al.*, 2004) because these rocks lie on an olivine control line along which liquids of roughly constant composition (with ~6–7 wt % MgO) are variably affected by olivine accumulation (Rhodes & Vollinger, 2004) and because they are compositionally distinct from higher SiO_2 bulk compositions used in previous experiments on Hawaiian lavas (e.g. Eggins, 1992; Wagner & Grove, 1998). We selected 25 wt % MgO for the bulk composition to ensure a large olivine primary phase volume with magnesian liquids and then computed corresponding values for 11 additional major and minor oxides from linear least-squares fits of oxide–MgO variations along the array of 'low-SiO_2' basalts. The resulting target composition, HP-25, is listed in Table 1. Numerous 1 atm

Table 1: Starting composition

	SiO_2	TiO_2	Al_2O_3	Cr_2O_3	FeO*	MnO	MgO	CaO	Na_2O	K_2O	P_2O_5	NiO
HP-25**	45·15	1·40	7·51	0·217	11·97	0·179	25·34	6·68	1·18	0·075	0·133	0·155
Syn-HP1†	45·72	1·42	7·61	0·219	12·12	0·182	25·67	6·77	0	0	0	0·292

**Mauna Kea picrite composition calculated from unweighted linear regression equations for bulk-rock major- and minor oxides versus MgO and an MgO value of 25; bulk-rock data from Rhodes & Vollinger (2004). The reported composition is normalized to 100 wt % with all Fe as FeO (FeO*), which leads to MgO slightly greater than 25.
†Syn-HP1 represents the HP-25 composition after increasing the NiO by 0·133 (the wt % of P_2O_5 in HP-25) and then renormalizing the composition on an Na_2O-, K_2O-, and P_2O_5-free basis.

experimental studies have shown that Na_2O, K_2O, and P_2O_5 display varying degrees of volatility at high temperatures (Corrigan & Gibb, 1979; Tsuchiyama *et al.*, 1981; Kilinc *et al.*, 1983; Yu *et al.*, 2003), so we left these three oxides out of the Syn-HP1 composition. In addition, we increased the NiO content in the synthetic composition relative to the HP-25 target composition by a small amount to facilitate measurement of NiO in the experimental glasses. It should be noted that all the experiments reported here were performed on the alkali- and P-free Syn-HP1 composition (in the Discussion section, we address the issue of applying our results to alkali-bearing tholeiitic magmas). The MgO content on the array of 'low-SiO_2' Mauna Kea basalts chosen for this study was a compromise between the desire for an MgO-rich starting composition with a broad range of olivine stability and the more practical goal of keeping the liquidus within the normal operational limits of our gas-mixing furnaces. Based on MELTS (Ghiorso & Sack, 1995) calculations, the selected alkali- and phosphorus-free nominal composition Syn-HP1 (Table 1) has a 1 atm liquidus at QFM of 1535°C.

A starting mix was prepared from high-purity oxides and carbonates ground for ~5 h under ethanol in an automated alumina mortar. After decarbonation, splits of the resulting powder were reduced for ~1 h at ~900°C at QFM using flowing H_2–CO_2 gas mixtures and a Pt catalyst to facilitate equilibrium within the gas (Beckett & Mendybaev, 1997). The reduced powder, as well as an unreduced split, were pressed into ~0·4 cm thick, 1·27 cm diameter pellets using ethanol as a binder. Chips weighing 60–100 mg were broken from these pellets and used in the experiments. Analyses of glass from a superliquidus experiment (run 43) show that the oxide mix gained ~0·7 wt % alumina through the grinding process. Minor Na_2O (0·05 wt %) was also present in this glass and low levels of Na_2O were detected in nearly all our experimental glasses. The presence and amounts of Na in the glasses observed in this nominally Na-free bulk composition are discussed below. Weight per cent values of the other oxides overlap those of the target composition at the 1σ level.

Experimental techniques

The 1 atm experiments were conducted in a vertical Deltech furnace at roughly 50°C intervals between 1300 and 1600°C using H_2–CO_2 gas mixtures to control fO_2. Temperature was monitored using a type-S thermocouple placed in the hot spot of the furnace and calibrated at the boiling point of water and the melting point of gold referenced to ITS_{90} (Goldberg & Weir, 1992). Most of the experiments were conducted at QFM as fO_2 estimates for Hawaiian magmas generally lie at or somewhat more reducing than this buffer (e.g. Rhodes & Vollinger, 2005). However, experiments were also run at the NNO buffer and under a continuous flow of air to examine the effect of fO_2 on the olivine–liquid Fe^{2+}–Mg exchange coefficient. For the purpose of guiding our choice of particular experimental fO_2 values, we used expressions for the QFM and NNO buffers from the compilation of Huebner (1971). Except for the superliquidus runs, the fO_2 was monitored using an yttria-stabilized zirconia oxygen sensor (SIRO2; Ceramic Oxide Fabricators, Eaglehawk, Australia) calibrated at the IW buffer (Huebner, 1971). For the two superliquidus runs, the gas mixture was adjusted with the aid of an oxygen sensor to yield the appropriate fO_2 at each run temperature, but the oxygen sensor was not present in the furnace during the run. Samples were suspended on 0·2 mm diameter FePt alloy loops using polyvinyl alcohol as a binding agent. Experiments were initiated by introducing the sample into the hot spot of the furnace at ~1100°C under a mixture of H_2–CO_2 set to provide the fO_2 of interest at the final run temperature. The furnace was then ramped to the desired temperature at 400–500°C h^{-1} (this initial ramp up is not included in the reported run times). Experiments were terminated by drop quenching the wire loop and attached sample into de-ionized water. Although no quench crystals were observed in our experimental glasses, thin (<1 μm) overgrowths were present on the olivines.

Even under the relatively oxidizing conditions of QFM, considerable Fe and Ni can be lost from a sample to a Pt loop (e.g. Hart & Davis, 1978; Grove, 1981). We therefore preconditioned loops by first conducting three to four 24 h

Table 2: Run conditions and experimental results

Run no.	T (°C)	Time (h)	log fO_2	Loop no. & usage**	ΔFeO* (%)†	ΔNa_2O (wt %)‡	Phase products	Phase proportions§
43	1600	0·5	−4·7¶	8/6	—	0·05	gl	100
34	1551	5·0	−5·1¶	8/5	—	b.d.l.	gl	100
26	1500	12·4	−5·51	6/3	0·8	0·22	gl, oliv	93·3(5), 6·8(6)
24	1451	24·9	−5·93	5/4	−2·2	0·22	gl, oliv	83·6(4), 16·4(6)
21	1452	48·2	−5·92	5/3	−5·2	0·25	gl, oliv	83·5(4), 16·5(6)
17	1401	48·2	−6·38	4/3	−2·6	0·39	gl, oliv	76·3(4), 23·7(5)
27	1398	24·9	−6·39	4/4	−3·3	0·05	gl, oliv	77·1(4), 22·9(6)
39	1396	50·1	−0·68	7/3	0·3	0·34	gl, oliv	83·1(4), 16·9(6)
28	1350	48·5	−5·99	2/4	0·3	0·04	gl, oliv, sp	70·7(3), 29·2(5), 0·10(3)
15	1349	66·7	−6·87	2/3	−2·2	0·41	gl, oliv, sp	69·2(3), 30·7(5), 0·10(3)
6	1302	22·3	−7·36	1/4	−6·4	0·22	gl, oliv, sp	63·4(3), 36·4(5), 0·16(2)
46	1300	48·1	−7·41	1/9	0·5	0·05	gl, oliv, sp	64·0(3), 35·8(4), 0·13(2)
8	1302	72·0	−7·36	1/5	−0·4	0·30	gl, oliv, sp	63·3(3), 36·6(5), 0·15(3)

All runs except numbers 28 and 39 were conducted at ~QFM. The oxygen fugacity of run 28 was held at ~NNO, whereas run 39 was equilibrated in air. gl, glass (quenched liquid); ol, olivine; sp, spinel.
**First number is the loop designation number; second value is the number of experiments that had been run with the loop prior to the present experiment.
†Relative change (in per cent) of FeO* in the bulk composition based on mass balance; negative sign denotes a decrease in FeO*.
‡Calculated addition of Na_2O (in wt %) to the bulk composition based on the sodium content of the glass and mass balance. Na_2O in run 34 was below the detection limit (b.d.l.).
§Phase proportions (in wt %) in all subliquidus experiments are given in the same order as listed in the phase products column. Numbers in parentheses are uncertainties in terms of the least units cited [e.g. 0·10(3) corresponds to $0{\cdot}10 \pm 0{\cdot}03$, where 0·03 is one standard deviation]. Uncertainties were estimated using the method of Albarède & Provost (1977) after the sodium and iron gain or loss was calculated for each experiment.
¶Oxygen fugacity was not measured during the superliquidus runs to prevent sensor degradation at these high temperatures. The gas mixture was set, at a lower T, to a value that would yield the desired fO_2 at the actual run temperature.

doping runs using Syn-HPl at the same temperature and fO_2 as desired for the first experiment that the loop was to be used for. At the end of each pre-saturation run, the sample was dissolved off the loop using an ~1:1 mixture (by volume) of HF and HNO_3. Once preconditioned, a loop was then used for one or more experiments conducted at the same conditions, except for loop 8, which was used at both 1551 and 1600°C. Table 2 lists the loop used for each experiment and the combined number of doping runs and experiments that had previously been run on it. Run times for experiments at a given temperature and fO_2 ranged from 72 h at 1300°C to 0·5 h at 1600°C. Chips from each experiment were broken off the loop, mounted in epoxy, and polished for electron microprobe analysis. Temperatures, fO_2 values, run times, observed phases, and their proportions calculated by mass balance (see below and footnote to Table 2) are also reported in Table 2.

Analytical techniques

Glass and crystalline phases produced in the experiments were analyzed with a five-spectrometer JEOL JXA-8200 electron microprobe at Caltech and all data were reduced using a modified ZAF procedure (CITZAF; Armstrong, 1988).

Quenched glasses were analyzed using a 15 keV accelerating voltage, 10 nA beam current, 10 μm spot, and glass, mineral, and oxide standards. Approximately 10 glass analyses were collected for each experiment. Counting times typically ranged from 20 to 40 s on peak and half that at high and low backgrounds. On-peak counting times on glasses from runs 43 and 46 were slightly longer for most elements and 100 s for Ni. Secondary glass standards (BHVO-2g, BIR-1g, and BCR-2g) were all analyzed during three separate periods during each microprobe session for a total of 9–12 points each. The mean BHVO-2g composition from each session coupled with the accepted composition of BHVO-2 (http://minerals.cr.usgs.gov/geochem_stand/) was used to reprocess the k-ratios for all glass analyses from a session; post-correction compositions of BIR-1g and BCR-2g overlap their accepted bulk-rock compositions (http://minerals.cr.usgs.gov/geo_chem_stand/). Glass analyses reported in Table 3 were accepted

Table 3: Phase compositions

Run	Phase	SiO_2	TiO_2	Al_2O_3	Cr_2O_3	FeO*	MnO	MgO	CaO	NiO	Na_2O	Sum
43	gl	46·19(23)	1·38(2)	8·32(7)	0·20(2)	11·95(14)	0·16(3)	25·59(14)	6·79(2)	0·22(1)	0·05(1)	100·87
34	gl	45·87(22)	1·42(2)	8·35(9)	0·21(2)	11·65(19)	0·15(3)	25·89(10)	6·83(3)	0·17(3)	b.d.l.	100·59
26	gl	46·33(20)	1·49(3)	8·80(7)	0·19(2)	12·31(23)	0·17(3)	23·90(14)	7·36(5)	0·18(5)	0·09(4)	100·85
26	ol	41·30(14)	0·01(1)	0·09(2)	0·09(1)	7·52(8)	0·10(1)	50·53(16)	0·21(1)	0·65(1)	—	100·51
24	gl	47·35(31)	1·64(2)	9·92(8)	0·21(1)	12·31(20)	0·17(2)	20·76(9)	8·13(7)	0·14(2)	0·16(3)	100·81
24	ol	41·28(14)	0·01(1)	0·10(1)	0·11(1)	8·64(7)	0·10(1)	49·93(19)	0·23(1)	0·61(2)	—	101·02
21	gl	47·10(25)	1·67(4)	9·96(9)	0·19(1)	11·8(2)	0·16(3)	21·04(14)	8·18(4)	0·15(4)	0·29(4)	100·57
21	ol	41·00(12)	0·01(1)	0·10(2)	0·10(1)	8·39(7)	0·11(1)	49·94(13)	0·22(1)	0·58(1)	—	100·45
17	gl	48·06(26)	1·81(4)	10·78(9)	0·21(1)	12·35(20)	0·18(4)	18·11(8)	8·86(5)	0·11(2)	0·51(3)	101·01
17	ol	40·94(15)	0·02(1)	0·10(2)	0·12(1)	9·62(8)	0·12(1)	49·12(10)	0·25(1)	0·59(2)	—	100·89
27	gl	47·87(28)	1·80(3)	10·64(6)	0·23(2)	12·01(26)	0·16(3)	18·41(20)	8·81(4)	0·13(3)	0·08(2)	100·17
27	ol	40·76(14)	0·02(1)	0·09(1)	0·12(1)	9·74(8)	0·12(1)	48·49(24)	0·23(1)	0·65(2)	—	100·20
39	gl	46·71(23)	1·67(4)	9·86(10)	b.d.l.	13·80(16)	0·17(3)	19·51(16)	8·15(5)	0·15(3)	0·40(4)	100·45
39	ol	42·22(10)	0·01(1)	0·11(1)	b.d.l.	3·05(4)	0·10(1)	54·68(13)	0·16(1)	0·91(3)	—	101·24
28	gl	48·40(27)	1·95(5)	11·47(7)	0·18(2)	12·45(23)	0·17(3)	15·95(13)	9·63(4)	0·11(4)	0·05(3)	100·36
28	ol	40·48(9)	0·02(1)	0·15(11)	0·11(1)	10·73(11)	0·13(1)	47·70(23)	0·26(3)	0·80(1)	—	100·39
28	sp	0·14(3)	1·07(2)	17·39(22)	45·43(67)	19·70(12)	0·20(4)	14·80(14)	—	0·51(2)	—	99·24
15	gl	48·78(18)	1·97(3)	11·89(8)	0·19(2)	12·23(24)	0·16(3)	15·40(12)	9·73(6)	0·09(3)	0·60(4)	101·07
15	ol	40·82(12)	0·01(1)	0·09(1)	0·12(1)	10·87(8)	0·14(1)	48·27(12)	0·25(1)	0·60(2)	—	101·17
15	sp	0·0	1·12(5)	18·7(4)	47·3(1·0)	17·45(14)	0·22(3)	14·4(9)	—	0·34(3)	—	99·23
6	gl	49·84(14)	2·18(4)	13·15(10)	0·15(1)	10·86(16)	0·16(3)	13·20(12)	10·58(7)	0·09(3)	0·35(3)	100·56
6	ol	40·33(19)	0·03(1)	0·09(1)	0·11(1)	11·51(13)	0·15(1)	47·38(20)	0·27(1)	0·53(2)	—	100·38
6	sp	0·0	1·20(5)	20·7(1·4)	44·8(1·7)	17·54(16)	0·21(2)	14·74(49)	—	0·31(2)	—	98·86
8	gl	49·18(28)	2·21(3)	12·74(13)	0·16(2)	11·65(16)	0·16(2)	13·37(10)	10·69(7)	0·08(4)	0·48(5)	100·74
8	ol	40·26(15)	0·03(1)	0·08(2)	0·10(1)	12·17(11)	0·15(1)	46·87(12)	0·27(1)	0·55(2)	—	100·47
8	sp	0·0	1·23(1)	19·7(6)	45·0(4)	18·48(10)	0·22(2)	14·43(34)	—	0·33(3)	—	99·184
6	gl	49·18(17)	2·16(2)	12·80(9)	0·16(2)	11·99(7)	0·17(2)	14·01(11)	10·51(3)	0·07(1)	0·07(1)	101·13
46	ol	40·69(29)	0·03(1)	0·07(3)	0·12(1)	12·03(5)	0·14(1)	46·9(3)	0·26(2)	0·55(2)	—	100·83
46	sp	0·08(15)	1·22(3)	21·0(6)	43·71(3)	17·69(11)	0·22(2)	15·1(4)	—	0·31(3)	—	99·33

All compositions listed in wt %. gl, glass; ol, olivine; sp, spinel. Numbers in parentheses are analytical uncertainties in terms of the least units cited [46·19(23) corresponds to $46{\cdot}19 \pm 0{\cdot}23$ where 0·23 is one standard sample deviation]; when the error is $\geq$1·0, we include the decimal point. FeO*, all Fe as FeO. —, not analyzed; b.d.l., below detection limit. K_2O in the glass was measured but below detection limits for all but one of our experiments. Run 21 had $0{\cdot}03 \pm 0{\cdot}02$ wt % K_2O. Spinel compositions in runs 15, 6, and 8 were corrected for fluorescence and beam overlap onto adjacent glass and/or olivine (spinels in these three runs are $<10\,\mu m$ in diameter). The silica content of the spinel was used as a proxy for the extent of glass and/or olivine 'contamination'. The average compositions of olivine and glass (in wt %) were subtracted from each spinel analysis so as to minimize the sum of $(SiO_2^{sp})^2 + (2 - B)^2 + (1 - A)^2 + (100 - \Sigma)^2$, where A and B are the sum of the cations in the A and B sites of an AB_2O_4 spinel, respectively, and Σ is the oxide wt % sum of the spinel analysis (including calculated Fe_2O_3). Thus, the silica content of average spinel in these three runs is zero. In each of these runs, the average corrected spinel composition overlaps with the small number of low-silica spinel analyses (<0·5 wt % SiO_2) suggesting that our correction procedure does not introduce a compositional bias. Glass FeO contents, measured by wet chemistry (Wilson, 1960), in runs 26 and 39 are 10·51(10) and 3·08(10) wt % respectively. The 1σ uncertainty in parenthesis is based on replicate analyses of secondary standards.

if their post-correction totals were between 98·5 and 101·5 wt %.

Experimentally produced olivines were analyzed using a 15 keV accelerating voltage, 40 nA beam current, 1 μm diameter spot size, and mineral and oxide standards. Counting times were 20–60 s on peak, and 10–30 s each on high and low backgrounds. In general, 10 olivine grains were analyzed from each charge. Most olivines have cross-sections of 25–100 μm in longest dimension and, for these, a single analysis was generally taken from

the central portion of the grain. Run 39 produced large (~250 μm) olivines, and for this experiment both core and rim analyses were collected; these indicate that the olivine grains in this run product are homogeneous at the 2σ level. To help remove inter-session variability, olivine analyses from a given probe session were referenced to the mean of multiple (7–28) analyses of San Carlos olivine obtained during the session. The occasional olivine analysis showing obvious signs of contamination (e.g. $Al_2O_3 > 1$ wt %) was rejected. The remaining olivine analyses were accepted if they had (1) an oxide total of $100 \pm 1{\cdot}5$ wt % and (2) a cation sum (on a four oxygen basis) of $3{\cdot}000 \pm 0{\cdot}015$. The data reported in Table 3 are averages of all olivine analyses from a given experiment that passed through these filters.

Spinels were analyzed using a 15 keV accelerating voltage, 25 nA beam current, a focused beam (nominal spot size of ~0·2 μm), and mineral and synthetic oxide standards. Peak counting times were 30 s with 15 s on high and low backgrounds. We analyzed 7–12 spinels in each run product containing this phase; most of these analyses were contaminated by adjacent phases owing to their small sizes (e.g. ~3 μm in diameter at 1300°C and ~9 μm at 1350°C). We used SiO_2 contents, which show a rough negative correlation with apparent grain size, as a measure of 'contamination'. After calculating Fe^{2+} and Fe^{3+} assuming ideal R_3O_4 stoichiometry, we accepted spinel analyses from runs 28 and 46 with ≤0·5 wt % SiO_2 and $2{\cdot}000 \pm 0{\cdot}015$ cations in the octahedral site. In runs 6, 8, and 15 only a few spinel analyses contained ≤0·5 wt % SiO_2 and so for these we corrected the spinel analyses for contamination from the coexisting glass and/or olivine (details are given in the notes to Table 3).

EXPERIMENTAL RESULTS

The temperature, run duration, fO_2, and phase assemblage of each experiment are reported in Table 2. Also listed are phase proportions and estimated changes in bulk Na and Fe (discussed below). Phase compositions are reported in Table 3.

Phase compositions

Olivine

Olivine is observed in all subliquidus experiments. For experiments conducted along the QFM buffer, the Fo content of olivine [100 × Mg/(Mg + Fe), atomic] increases monotonically with increasing temperature from 87·3 at ~1300°C to 92·3 at 1500°C. Olivine from the air-equilibrated experiment, performed at 1396°C, is much more magnesian than that in comparable QFM experiments ($Fo_{97{\cdot}0}$ vs $Fo_{90{\cdot}0}$), whereas olivine from the NNO experiment, performed at 1350°C, has a nearly identical Fo content to that in the comparable QFM experiment ($Fo_{88{\cdot}8}$). In the experiments conducted at QFM, concentrations of MnO (0·10–0·15 wt %) and CaO (0·21–0·28 wt %) in olivine decrease slightly with increasing temperature; concentrations of Al_2O_3 and Cr_2O_3 are constant within error (0·07–0·11 and 0·09–0·12 wt %); and NiO contents (0·53–0·65 wt %) increase with temperature. The Cr, Mn, and Al olivine–liquid partition coefficients obtained in our experiments agree well with other experimental studies (e.g. Mäkipää, 1980; Murck & Campbell, 1986; Agee & Walker, 1990; Parman *et al.*, 1997; Hanson & Jones, 1998; Bédard, 2005), and the Ca olivine–liquid partition coefficients are similar to the results of previous studies and the predictions of Libourel (1999), keeping in mind that no effort was made in this study to correct olivine analyses for the fluorescence of Ca from adjacent glass.

Spinel

The experiments at 1300–1350°C contain small amounts of Al-rich chromite (<0·2 wt %; Table 2) in addition to glass and olivine. Despite their low abundance, the spinels account for as much as 36% of the Cr budget in these experiments; Cr-number [Cr/(Cr + Al), atomic], ranges from 0·59–0·64 in the spinels. Fe^{3+}/Fe^* (Fe^* is all Fe as Fe^{2+}) ratios calculated assuming an R_3O_4 stoichiometry are between 0·24 and 0·26 for the QFM experiments, but they are distinctly higher, 0·37, in the NNO run (no. 28). TiO_2 contents (1·1–1·2 wt %), Cr-numbers, and Mg-numbers (0·65–0·68) of the experimental spinels are comparable with those observed in spinels from Hawaiian lavas (e.g. Clague *et al.*, 1995; Baker *et al.*, 1996; Kamenetsky *et al.*, 2001; Roeder *et al.*, 2003).

Glass

Figure 1 shows concentrations of selected oxides from the experimental glasses as a function of temperature. Taking the QFM and NNO data together, concentrations of SiO_2, TiO_2, and MgO in the glass are monotonic functions of temperature (as are concentrations of Al_2O_3 and CaO, which are not shown), reflecting the absence of major crystalline phases other than olivine. FeO* contents of the QFM glasses are essentially independent of temperature, reflecting the similar FeO* contents of olivine and glass in these experiments (Fig. 1d; note the FeO* plot is noisier than for other oxides as a result of the minor Fe loss or gain in these experiments). The glass from the air experiment (run 39) plots off the trends for all oxides shown in Fig. 1 owing to the high Fe^{3+}/Fe^{2+} in the glass (e.g. Kilinc *et al.*, 1983) and the correspondingly Fe^{2+}-poor coexisting olivine.

Figure 1c shows that MgO contents of the olivine-bearing experimental glasses at QFM and NNO are approximately linear as a function of temperature; an unweighted least-squares fit to our QFM data yields $T(^\circ\mathrm{C}) = 19{\cdot}2 \times (\mathrm{MgO,\ wt\ \%}) + 1048$. The slope (~19) is similar to values (16–23) calculated using 1 atm

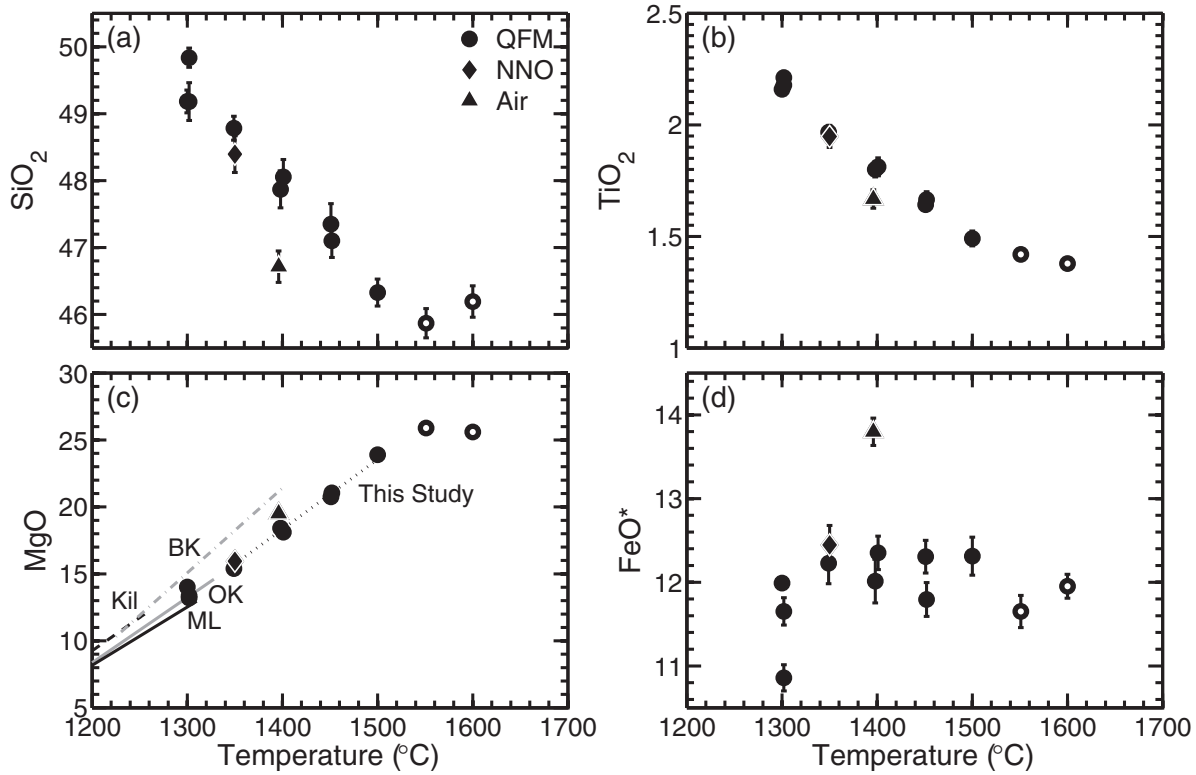

Fig. 1. Concentrations of oxides (wt %) in the experimental glasses as a function of run temperature (°C). Symbol indicates the oxygen fugacity; open circles for the 1550 and 1600°C data indicate superliquidus experiments. Error bars represent one standard deviation and, where not visible, are smaller than the size of the symbols. (a) SiO_2. (b) TiO_2. (c) MgO. Lines are for MgO–T(°C) regressions from this study, for Kilauea (Kil) and Mauna Loa (ML) basalts by Helz & Thornber (1987) and Montierth *et al.* (1995), and for Barberton (BK) and Ontario (OK) komatiites by Thy (1995) and Parman *et al.* (1997). (d) FeO*, all Fe as FeO.

experiments on Hawaiian basaltic compositions (Helz & Thornber, 1987; Montierth *et al.*, 1995) and komatiitic compositions (Thy, 1995; Parman *et al.*, 1997) (see Fig. 1c). Transforming the T(K) vs mol % MgO global fit of olivine-saturated 1 atm experiments given by Sugawara (2000) into T(°C) vs wt % MgO space yields a slope of ~17·8 (for liquids with ~2 to 26 wt % MgO). It should be noted that liquids from the highest temperature experiments for the Hawaiian studies (1261°C, Helz & Thornber, 1987; 1310°C, Montierth *et al.*, 1995) contained 1·7–2 wt % Na_2O. The fact that our glasses with much lower alkali contents yield a trend line with a similar slope to the more Na + K-rich Hawaiian data suggests that sodium values between ~0·1 and ~2 wt % have little effect on these trends and that the expression derived from our data is applicable to a broad range of liquid compositions. In a recent study, Putirka (2008*b*) obtained a higher slope (26) for the Mg-in-glass thermometer than reported by other workers. This reflects the use by Putirka (2008*b*) of both high- and low-pressure data from the LEPR database (Hirschmann *et al.*, 2008) without including a pressure term in the equation. Considering only the 1 atm experiments in the LEPR database yields a slope of 18·1, consistent with values obtained by previous workers.

Two elements, Na and Cr, were affected by volatility during our experiments. Although no sodium was added to our starting mix and care was taken to avoid inadvertent sodium addition during its preparation, all but one of our glasses contain Na concentrations above background, with abundances of 0·05–0·6 wt % (Table 3). We believe that these relatively small amounts of Na were acquired through re-volatilization, either deposited by previous Na-bearing experiments or as a contaminant on new furnace tubes. The concentration of Na_2O in our experimental glasses declined with each successive experiment unless temperature was increased, thereby accessing Na further from the hot spot. This suggests a gradual depletion of Na from the inner wall of the Al_2O_3 furnace tube as the reservoir of Na on the inner tube surface was depleted. We analyzed glasses for K_2O and P_2O_5 but concentrations of these oxides were negligible (see notes for Table 3). Generally, Cr was conserved during experiments; however, the 1400°C run in air lost nearly all of its Cr owing to volatility under oxidizing conditions (Hanson & Jones, 1998).

Experiments run under the same conditions but for different times provide information on the approach to equilibrium in the experiments. For example, we conducted two QFM experiments each at ~1400°C and ~1450°C (25 and 48 h), and three at ~1300°C (22, 48, and 72 h). Although there are differences in the concentrations of Na_2O in glasses run at similar conditions but for different durations (reflecting, as discussed above, re-mobilization of previously deposited or condensed Na on the alumina furnace tubes), for the most part all other oxide concentrations in the glasses overlap at the 2σ level in each time series. Exceptions (in the 1300°C experiments) largely reflect variable amounts of Fe loss or gain, but even in these cases we infer that exchange equilibrium between olivine and liquid was closely approached, given that values of $K_{D,Fe^{2+}-Mg}$ within each time series, including the one at 1300°C, overlap at the 1σ level.

Phase proportions

The proportions of phases in subliquidus experiments were determined by mass balance using the non-linear approach of Albarède & Provost (1977), which incorporates uncertainties on the bulk and phase compositions. The analyzed glass from superliquidus run 43 (1600°C) was taken as representative of the bulk composition [except for the air experiment, where the bulk Cr_2O_3 was set equal to zero; using run 34 (1551°C) for these calculations yields virtually identical results]. We included FeO*, Na_2O, and NiO as variables in the bulk composition because these components may have varied and, according to our calculations, did vary from experiment to experiment. The oxide sum of the bulk composition was held constant, and any changes in the bulk concentrations of FeO*, Na_2O, or NiO required to minimize χ^2 were compensated by corresponding proportional changes to concentrations of all the remaining oxides (with 10 equations and either five or six—if spinel is present—unknowns, our mass-balance problems are still over-determined). All experiments yielded mass-balance solutions acceptable at the 95% confidence level (i.e. goodness of fit values, $Q \geq 0{\cdot}05$; see Press *et al.*, 1992). Our mass-balance calculations suggest that loop preconditioning was successful in limiting iron loss to the Pt wire; bulk FeO changed by −6·4% (loss) to +1·5% (gain) with most in the range −2·2 to +1·5 % (relative).

The proportions of liquid and olivine in our experiments are plotted in Fig. 2a as functions of temperature for the ~QFM data with quadratic fits for each phase. The weight per cent of liquid steadily increases and that of olivine decreases with increasing temperature until, at 1538°C according to the second-order polynomial fit of the olivine mode, the bulk composition is at the liquidus. This predicted liquidus temperature is consistent with our experimental constraint that the bulk composition is above the liquidus at 1551°C and below it at 1500°C and with the prediction of 1531°C for the 'as analyzed' bulk composition (run 43; Table 3) obtained from MELTS (which is also similar to the 1535°C value cited above for the nominal alkali-free version of this bulk composition; Table 1). Although the olivine content was fitted to a quadratic, the slope of the olivine vs temperature curve in Fig. 2a is relatively constant at ~0·14 wt % $^{\circ}C^{-1}$ over the range of our experiments. Fits to modes in the olivine primary phase field from the 1 atm experiments of Thy (1995) and Parman *et al.* (1997) on komatiitic compositions (16 and 23 wt % MgO), yield similar slopes of ~0·15 and ~0·14 wt % $^{\circ}C^{-1}$. Although not shown in Fig. 2a, modes from the MELTS calculations (Ghiorso & Sack, 1995; Smith & Asimow, 2005) are almost indistinguishable from the quadratic fits in Fig. 2a.

Increasing oxygen fugacity at constant temperature suppresses olivine crystallization in Syn-HPl; for example, there is 1·5 wt % less olivine at NNO and 1350°C than there is at QFM and 6·4 wt % less olivine at 1396°C in air than there is at QFM at 1400°C. Although the best-fit olivine proportions in the NNO and QFM experiments at ~1350°C overlap at 2σ (see Table 2), the difference in the modes is in the same direction as that seen in the air and QFM experiments at ~1400°C. This effect can also be seen in simple systems such as MgO–FeO–SiO_2–O_2 (e.g. Muan & Osborn, 1956) in which olivine–liquid tie lines for a given temperature must rotate and extend towards more magnesian olivine compositions with increasing fO_2. Because the position of the liquidus isotherm is a relatively weak function of fO_2, the lever principle dictates that the olivine/liquid ratio for a given bulk composition decreases with increasing fO_2. This destabilization of olivine with increasing fO_2 is the flip side of the well-known stabilization of spinel in basaltic melts with increasing fO_2 (e.g. Hill & Roeder, 1974); both phases respond to increases in Fe^{3+}/Fe^{2+} in the melt as fO_2 is increased. For spinel, stabilization of magnetite and magnesioferrrite components in the spinel owing to increased activities of these components in the melt offsets any destabilization of Fe^{2+}-bearing components. Olivine, in contrast, has a negligible solubility for Fe^{3+} and, because $K_{D,Fe^{2+}-Mg}$ in air and QFM are nearly identical for Syn-HPl (Fig. 3 and discussion below), higher Fe^{3+}/Fe^{2+} in the melt translates into lower activities of the fayalite component in the melt and, therefore, higher Mg/Fe^{2+} in the coexisting olivine and this requires a decrease in the modal abundance of olivine. Figure 2b shows weight per cent liquid by mass balance for the ~1350 and ~1400°C experiments (Table 2) and spinel-suppressed MELTS calculations using the glass composition from run 43 (Table 3) at these two temperatures as a function of $\log fO_2$ relative to the QFM buffer. Both MELTS curves show an increase in liquid fraction with increasing fO_2 and, in particular, the 1350°C MELTS curve overlaps the liquid modes of our

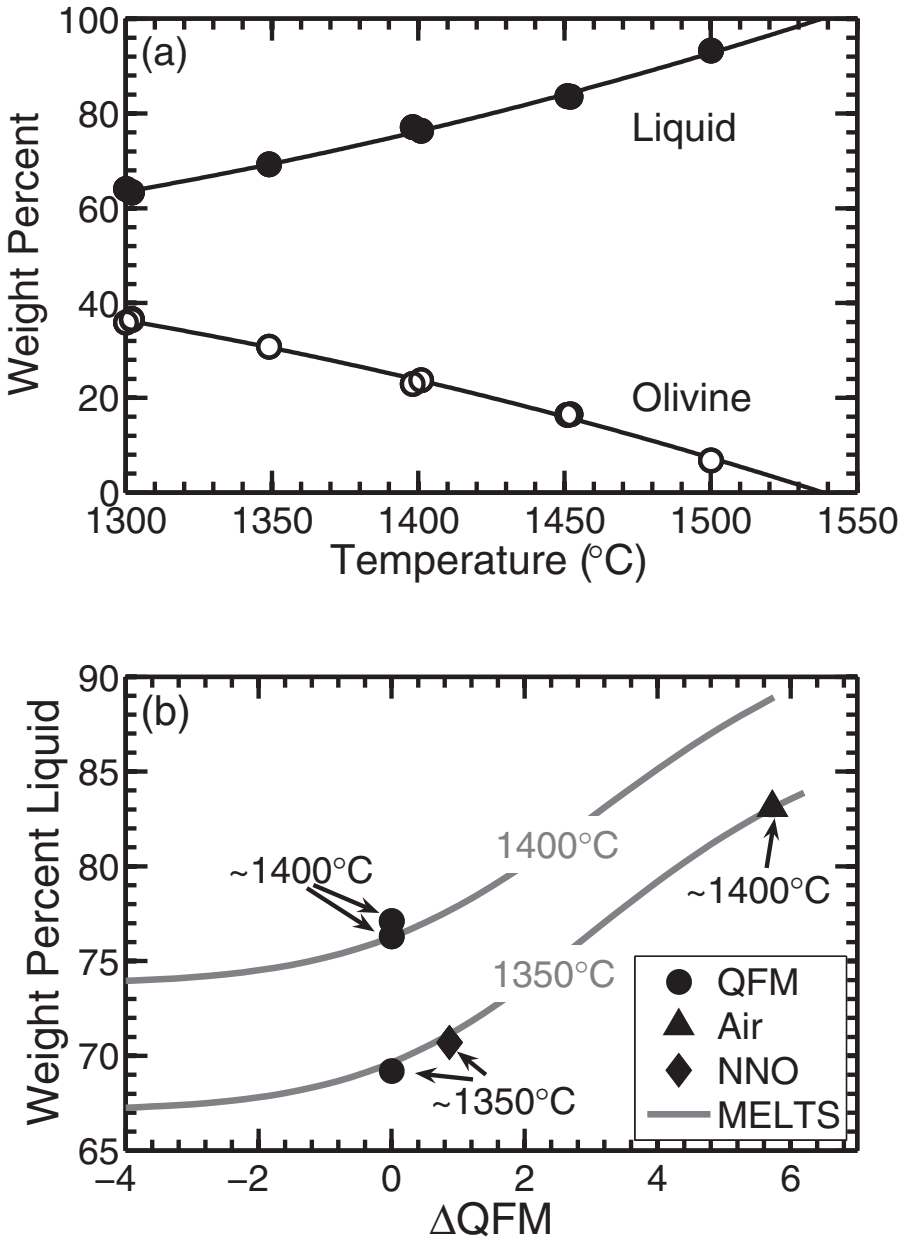

Fig. 2. (a) Weight per cent of liquid (closed symbols) and olivine (open symbols) determined by mass balance (Table 2) for ~QFM experiments. Continuous black curves are polynomial fits: liquid (wt %) = $243{\cdot}1 - 0{\cdot}3847(T) + 1{\cdot}896 \times 10^{-4}(T)^2$; olivine (wt %) = $-150{\cdot}4 + 0{\cdot}394(T) - 1{\cdot}925 \times 10^{-4}(T)^2$, where T is the temperature (in °C). Proportions of liquid and olivine as calculated by MELTS at QFM (with spinel suppressed; i.e. not allowed to crystallized) are not shown as they are virtually identical to our polynomial fits. (b) Weight per cent liquid vs deviation (ΔQFM) in $\log f\mathrm{O}_2$ from QFM (O'Neill, 1987) at the same temperature. Shape of the symbol indicates the oxygen fugacity of the experiment. The very slight offset of our QFM experiments from zero reflects differences between the QFM expression of Eugster & Wones (1962), which was quoted by Huebner (1971) and used to set the experimental conditions, and that of O'Neill (1987). MELTS calculations on our analyzed bulk composition (run 43, Table 3) at 1350 and 1400°C as a function of $f\mathrm{O}_2$ are shown by continuous gray curves. Spinel was suppressed in the MELTS calculations because the program predicts substantially higher spinel modes (2–3 wt % in air at 1400°C) than are observed in our experiments (0·1–0·2 wt %).

1350°C QFM and NNO experiments (noting that typical 1σ errors from the mass balance for the liquid fraction are 0·3–0·4 wt %). At higher $f\mathrm{O}_2$ values, the MELTS curves are qualitatively consistent with our data. The Fo content of olivine predicted by MELTS is, however, higher at 1396°C in air than is observed in our experiment (98·4 vs 97·0), and the predicted MELTS $K_{\mathrm{D,Fe^{2+}-Mg}}$ is much lower (0·130 vs 0·353). We suspect that these differences

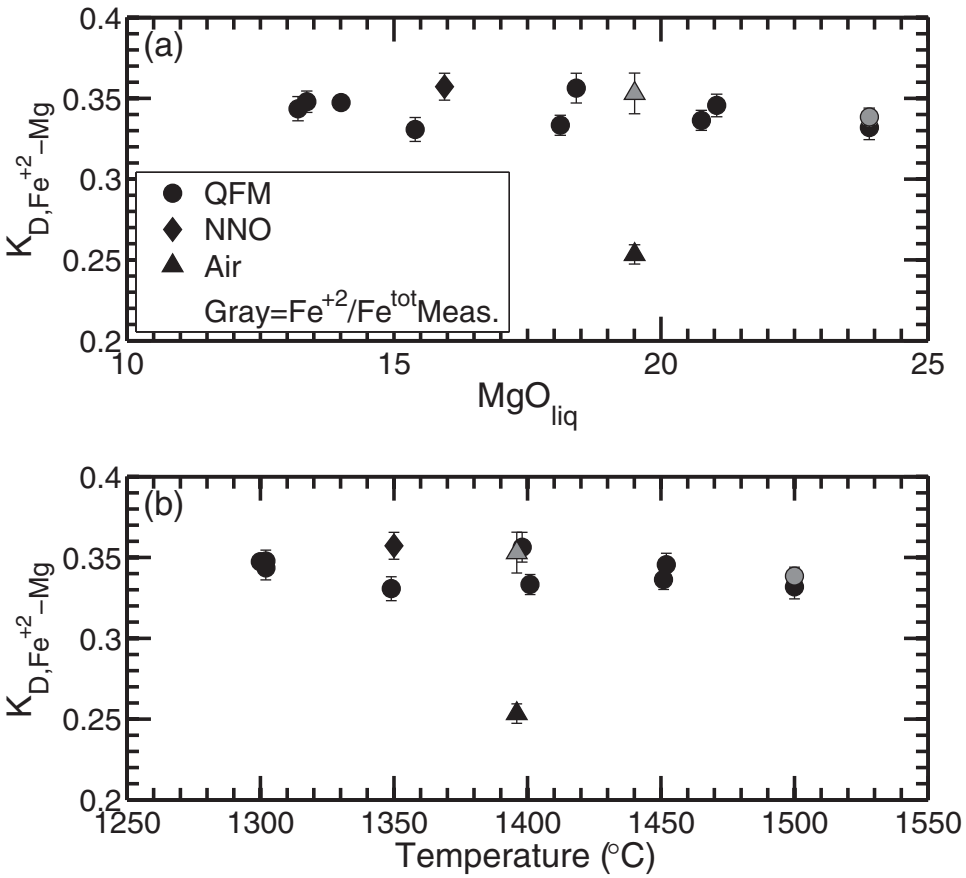

Fig. 3. Olivine–liquid $K_{D,Fe^{2+}-Mg}$ vs (a) MgO contents of the liquid and (b) temperature (°C). In both panels, symbol shape denotes the fO_2 of the experiment (see also the caption to Fig. 1) and black symbols indicate that Fe^{2+} in the liquid was calculated using equation (12) of Jayasuriya *et al.* (2004). Gray symbols represent experiments where the FeO content of the quenched liquid was measured by wet chemistry (see Table 3).

are, in part, related to the Fe^{3+}/Fe^{2+} equation of Kress & Carmichael (1991), which is used in MELTS.

Olivine–liquid Fe^{2+}–Mg exchange coefficients

Knowledge of the Fe^{2+} (or equivalently the FeO) content of an olivine-saturated liquid is a prerequisite for calculating $K_{D,Fe^{2+}-Mg}$. FeO contents of glasses can be measured by wet chemistry (e.g. Yokoyama & Nakamura, 2002), Mössbauer spectroscopy (e.g. Partzsch *et al.*, 2004), and/or XANES (X-ray absorption near edge structure) spectroscopy (e.g. Cottrell *et al.*, 2009); more often, however, parameterizations based on such measurements are used to calculate Fe^{3+}/Fe^{2+} as a function of temperature, fO_2, and liquid composition (e.g. Sack *et al.*, 1980; Kilinc *et al.*, 1983; Kress & Carmichael, 1991). In Fig. 3, we show calculated $K_{D,Fe^{2+}-Mg}$ values from our experiments as a function of liquid MgO content (Fig. 3a) and temperature (Fig. 3b): for the data points shown in black, we used the algorithm of Jayasuriya *et al.* [2004, equation (12)] to calculate Fe^{3+}/Fe^{2+} in the liquid; we justify the choice of this parameterization in the discussion below. For the two experiments shown in gray (runs at 1500°C and QFM and 1396°C in air), we have wet chemical determinations of the abundance of FeO in the glasses provided by R. A. Lange (see notes to Table 3), which lead to $K_{D,Fe^{2+}-Mg}$ values of $0{\cdot}338 \pm 0{\cdot}006$ and $0{\cdot}353 \pm 0{\cdot}013$, respectively. The 1σ error bars in Fig. 3 are based on Monte Carlo propagation of uncertainties on (1) the concentrations of FeO and MgO in the olivines as measured by electron microprobe (Table 3), (2) the concentrations of FeO* and MgO in the glasses as measured by electron microprobe (Table 3), and (3) the concentrations of FeO in the glasses as measured by R. A. Lange (see Table 3). For those experiments where we calculated FeO in the glasses using equation (12) of Jayasuriya *et al.* (2004), the Monte Carlo calculations assumed flat distributions of ± 3°C and $\pm 0{\cdot}05$ log units for fO_2, but we ignored the errors associated with the equation's fit parameters.

The data in Fig. 3 show that all of the $K_{D,Fe^{2+}-Mg}$ values, except for the air experiment calculated via Jayasuriya *et al.* (2004), are in the narrow range of 0·33–0·36 (the

unweighted average for all 11 experiments is $0{\cdot}345 \pm 0{\cdot}009$, 1σ; for runs 26 and 39, $K_{D,Fe^{2+}-Mg}$ values used to calculate this average were based on the FeO concentration in the glass as measured by wet chemistry). This mean $K_{D,Fe^{2+}-Mg}$ is substantially higher than the canonical value of 0·30 of Roeder & Emslie (1970). There is no statistically significant correlation (at the 95% confidence level) with either temperature (over a 200°C range, 1300–1500°C), consistent with Roeder & Emslie's observation at 1152–1266°C or MgO (over the interval of ~13 to 24 wt %; unless otherwise stated, statistical tests for correlation are based on the non-parameteric Spearman rank-order correlation coefficient, r_S; Press *et al.*, 1992). Thus, for this MgO-rich bulk composition, over the range of conditions we have studied, $K_{D,Fe^{2+}-Mg}$ appears to be independent of temperature, melt composition, and fO_2. The only significant discrepancy shown in Fig. 3 is between the two $K_{D,Fe^{2+}-Mg}$ values in air, one based on a wet chemical measurement of Fe^{2+} and the other based on a calculation of Fe^{3+}/Fe^{2+} ratio using the algorithm of Jayasuriya *et al.* (2004). Although we do not know the source of the discrepancy, it is unlikely to be olivine contamination of the glass separate analyzed by wet chemistry, as the measured FeO contents of the glass and olivine in the air experiment are nearly identical (3·08 and 3·05 wt %, respectively; Table 3), and thus any addition of olivine to the glass separate would have almost no effect on the wet chemical FeO measurement. We note that most of the other Fe^{3+}/Fe^{2+} models tested also predict a low $K_{D,Fe^{2+}-Mg}$ for our experiment in air—a discrepancy that is puzzling as all of the models published after Sack *et al.* (1980) include the air experiments of Kilinc *et al.* (1983), and the available air experiments cover a region of composition space (other than Fe^{3+}/Fe^{2+}) comparable with coverage for the more reducing experiments.

DISCUSSION

In their landmark study, Roeder & Emslie (1970) found for a range of basaltic bulk compositions that the logarithm of the partition coefficients for MgO and FeO between olivine and silicate melt are each a linear function of inverse temperature of roughly equal slope. Thus, when a ratio of the two partition coefficients is taken to form an exchange coefficient, $K_{D,Fe^{2+}-Mg}$, the temperature dependences of the partition coefficients essentially cancel, leaving $K_{D,Fe^{2+}-Mg} = 0{\cdot}30 \pm 0{\cdot}03$ (1σ), independent of both temperature and liquid composition. Subsequent experimental work (e.g. Sack *et al.*, 1987; Gee & Sack, 1988) demonstrated that $K_{D,Fe^{2+}-Mg}$ decreases with increasing alkali content in the melt, reaching values as low as 0·18 for highly nepheline- and/or leucite-normative bulk compositions. Moreover, Kushiro & Walter (1998) and Kushiro & Mysen (2002) found $K_{D,Fe^{2+}-Mg}$ values ranging from 0·25 to 0·35 (without correcting for the presence of Fe^{3+}), and noted that $K_{D,Fe^{2+}-Mg}$ correlates with the degree of polymerization of the melt as measured by NBO/T. In contrast, Toplis (2005) attributed most of the variation in $K_{D,Fe^{2+}-Mg}$ to variations in the silica and alkali contents of the coexisting liquids rather than to NBO/T. The essential point, however, is that $K_{D,Fe^{2+}-Mg}$ is a function of melt composition if a sufficiently large range is considered. In light of substantial variations in $K_{D,Fe^{2+}-Mg}$ apparent in the literature data and the discrepancy between $K_{D,Fe^{2+}-Mg}$ obtained through wet chemistry and the algorithm of Jayasuriya *et al.* (2004) for our air experiment, several questions arise in the context of our experiments: (1) Are our data for MgO-rich liquids consistent with previous 1 atm experiments from the literature? (2) How much does the choice of Fe^{3+}/Fe^{2+} algorithm affect the calculated $K_{D,Fe^{2+}-Mg}$ values from experiments conducted under fO_2 values most relevant for terrestrial basalts (i.e. ~QFM; Carmichael, 1991)? (3) Are there compositional ranges for basaltic melts (e.g. Hawaiian tholeiites or mid-ocean ridge basalts) over which $K_{D,Fe^{2+}-Mg}$ can be safely approximated to be constant?

Comparison of our data with exchange coefficients from literature-based olivine–liquid pairs

We assembled a comprehensive database of 1 atm experiments with coexisting olivine and glass analyses from the literature for comparison with our data. We chose not to consider high-pressure experiments in graphite capsules because, although these experiments are reducing (Médard *et al.*, 2008), the fO_2 values are not so low that Fe^{3+} can be ignored in calculating $K_{D,Fe^{2+}-Mg}$. Moreover, given the lack of oxygen buffers or independent measures of fO_2 in most of these experiments and the paucity of data on pressure corrections to Fe^{3+}/Fe^{2+} in the melt (O'Neill *et al.*, 2006), $K_{D,Fe^{2+}-Mg}$ is inherently less well constrained in graphite capsule experiments conducted at high pressures than it is in 1 atm experiments. All selected bulk compositions contain at least the elements Si, Al, Fe, Mg, and Ca and the majority resemble natural basalts. In an effort to remove low-quality analyses from the dataset, we applied the following compositional filters: oxide totals for glass of $100{\cdot}0 \pm 1{\cdot}5$ and olivine tetrahedral and total cation sums per four oxygens of $1{\cdot}000 \pm 0{\cdot}015$ and $3{\cdot}00 \pm 0{\cdot}015$, respectively. We also applied the following three compositional filters: olivine NiO and CoO contents <6 wt %, a conservative upper limit for Henry's law behavior (e.g. Mäkipää, 1980; Drake & Holloway, 1981) and TiO_2 contents of glass <6 wt %, as higher TiO_2 contents are known to affect $K_{D,Fe^{2+}-Mg}$ [Longhi *et al.*, 1978; see Xirouchakis *et al.* (2001) for a discussion of the effect of increasing TiO_2 on olivine–liquid $K_{D,Fe^{2+}-Mg}$ at constant silica activity]. The glass oxide sum constraint was applied to highly reduced experiments [$fO_2 \leq IW + 0{\cdot}5$; IW

buffer calculated using the equation of Huebner (1971)] based on the assumption that all Fe is present as FeO (i.e. FeO*); for more oxidized runs, this constraint was applied after first calculating FeO and Fe_2O_3 abundances using equation (12) of Jayasuriya *et al.* (2004). The 964 experiments (from our database of 1179 olivine–liquid pairs from the literature) that passed these filtering constraints span temperatures from 1009 to 1600°C and fO_2 values from ~IW − 3 to air (data references are given in the Supplementary Material available at http://www.petrology.oxfordjournals.org/). The Fo contents of the olivines in this dataset range from 28 to 99, and MgO contents in the glasses range from 1·3 to 28 wt %.

Olivine–liquid pairs in our literature dataset can be divided into three categories: (1) Fe^{3+}/Fe^{2+} in the liquid is known by direct measurement of the quenched glass; (2) Fe^{3+}/Fe^{2+} was not measured but run conditions were sufficiently reducing that Fe^{3+} can be neglected (e.g. at fO_2 values $\leq$ IW + 0·5 and 1 atm according to the model of Jayasuriya *et al.* (2004), molar Fe^{3+}/Fe^{*} is less than 0·035); (3) Fe^{3+}/Fe^{2+} was not measured but can be calculated using one of the algorithms developed for this purpose (e.g. Sack *et al.*, 1980; Kilinc *et al.*, 1983; Kress & Carmichael, 1991). Experiments in category 1 are ideally suited to answering the questions posed above, as calculated $K_{D,Fe^{2+}-Mg}$ values from these experiments are independent of any Fe^{3+}/Fe^{2+} algorithm. We are, however, aware of only 33 olivine-bearing experiments in the literature with reported Fe^{3+}/Fe^{2+} ratios (Mysen & Dubinsky, 2004; Partzsch *et al.*, 2004; Mysen & Shang, 2005; Mysen, 2006, 2007), 24 of which were performed in air, and of the nine remaining, only six were run at fO_2 values $\leq$ QFM. The 172 experiments in category 2 are dominated by Fe-rich bulk compositions with low total alkalis (range in olivine Fo-number is 33–96 with a median and mean absolute deviation of 72 ± 11; from this point on we refer to the mean absolute deviation as 'MAD'). We also constructed a dataset from category 3 experiments run within 0·25 log units of the QFM buffer, as defined by O'Neill (1987); the median Fo content of olivine in these 446 experiments is 79 ± 7 (MAD), with a range of 45–95. As most of our experiments were performed at QFM, this is a convenient dataset for comparing literature data with our experimental results. Because of the small number of category 1 experiments and their bias towards highly oxidizing conditions, we emphasize category 2 and 3 experiments in the following discussion.

To test the viability of treating all Fe as Fe^{2+} in the reduced experiments, we first computed Fe^{3+}/Fe^{2+} ratios in the melt by applying equation (12) of Jayasuriya *et al.* (2004) to experiments in the $\leq$ IW + 0·5 dataset. For Fe-capsule experiments, the required fO_2 values were calculated based on expressions from Snyder & Carmichael (1992) and Righter *et al.* (1997) and data from Robie *et al.* (1978) [using the iron activity model of Roeder (1974) instead of Snyder & Carmichael's has a negligible effect on the calculated fO_2 values]. These computations lead to a median $K_{D,Fe^{2+}-Mg}$ value of 0·34 ± 0·02 (MAD; the range in $K_{D,Fe^{2+}-Mg}$ values is 0·24–0·41). Assuming all Fe in the melt to be ferrous yields a median $K_{D,Fe^{2+}-Mg}$ of 0·33 ± 0·02 (MAD; range is 0·23–0·40) for the same experiments. Thus, the influence of Fe^{3+} in the melt on calculated $K_{D,Fe^{2+}-Mg}$ is small for these reduced experiments. To test the consistency of the $\leq$ IW + 0·5 dataset with the QFM ± 0·25 dataset, for which Fe^{3+}/Fe^{2+} cannot be ignored, we calculated Fe^{3+}/Fe^{2+} for the QFM ± 0·25 literature glasses using equation (12) of Jayasuriya *et al.* (2004), and then computed values of $K_{D,Fe^{2+}-Mg}$. The range of $K_{D,Fe^{2+}-Mg}$ values for the QFM ± 0·25 experiments is 0·13–0·41, with a median of 0·34 ± 0·03; again, the uncertainty given here is the mean absolute deviation. The median $K_{D,Fe^{2+}-Mg}$ values for both $\leq$ IW+0·5 (0·34 ± 0·02) and QFM ± 0·25 (0·34 ± 0·03; median and MAD, respectively) datasets overlap the mean $K_{D,Fe^{2+}-Mg}$ value calculated from our experiments (0·345 ± 0·009; mean and 1σ, all 11 experiments); indeed, they are essentially identical. The agreement is also good if we consider only the 78 glasses from the literature at QFM ± 0·25 with 46–52 wt % SiO_2, ≤3 wt % $Na_2O + K_2O$ and Fo_{92-80} olivines, bounds that overlap with our olivine-saturated experiments and incorporate most tholeiitic magmas (Le Maitre, 1976; Rhodes & Vollinger, 2004; Stolper *et al.*, 2004). The median $K_{D,Fe^{2+}-Mg}$ for these 78 olivine–liquid pairs is 0·340 ± 0·012 (MAD), a value essentially identical to the mean value of 0·343 ± 0·008 from our QFM experiments and to the median from the full QFM ± 0·25 literature dataset (0·34 ± 0·03). The agreement between our data and those in the literature that require no correction for the amount of Fe^{3+} in the melt and those that do require a correction is important in that it demonstrates a consistency between $K_{D,Fe^{2+}-Mg}$ values measured in the experiments presented here and a large number of 1 atm experiments from the literature. Moreover, this consistency in $K_{D,Fe^{2+}-Mg}$ spans a wide range of mafic to ultramafic liquid compositions and is significantly higher than the canonical value of 0·30. In the Supplementary Material, we explore possible reasons for the discrepancy between the canonical $K_{D,Fe^{2+}-Mg}$ value of 0·30 obtained by Roeder & Emslie (1970) and the higher values for our data and most of those in the literature. We also discuss predictions of the Ford *et al.* (1983) and Toplis (2005) models for $K_{D,Fe^{2+}-Mg}$.

Calculating Fe^{3+}/Fe^{2+} for a given liquid is a crucial step in obtaining an accurate $K_{D,Fe^{2+}-Mg}$. To assess how the different expressions for calculating Fe^{3+}/Fe^{2+} that are available in the literature affect calculated $K_{D,Fe^{2+}-Mg}$ values at terrestrially relevant fO_2 values, we calculated $K_{D,Fe^{2+}-Mg}$ values for glasses from the QFM ± 0·25 dataset

after first calculating FeO contents using each of the following eight parameterizations: Sack *et al.* (1980), Kilinc *et al.* (1983), Kress & Carmichael (1988), Borisov & Shapkin (1989), Kress & Carmichael (1991), Jayasuriya *et al.* (2004) equations (12) and (14), and Ghiorso & Kress (2004). However, comparing how these different parameterizations affect $K_{D,Fe^{2+}-Mg}$ is difficult, not only because the calculated Fe^{3+}/Fe^{2+} values are functions of liquid composition, but also because the resulting $K_{D,Fe^{2+}-Mg}$ values are correlated with both liquid and olivine composition. In an effort to minimize the compositional effects on $K_{D,Fe^{2+}-Mg}$ so that we could consider as large a body of olivine–liquid pairs as possible, we parameterized each dataset as a function of 'S', a component in the CMAS projection scheme ['S' = S/(C + M + A + S); Basaltic Volcanism Study Project 1981, chapter 3.3; Gee & Sack, 1988; see also the Supplementary Material], which we calculated on a molar basis. We used the expression $K_{D,Fe^{2+}-Mg} = a + b \times \exp(c \times \text{'S'})$ for this purpose, where a, b and c are least-squares fit parameters. Correlation coefficients for the fits range from 0·72 to 0·84, although most lie between 0·82 and 0·84. Gee & Sack (1988) showed that $K_{D,Fe^{2+}-Mg}$ is strongly correlated with 'S', which incorporates terms for Na_2O and K_2O in addition to SiO_2, and Toplis (2005) showed that $K_{D,Fe^{2+}-Mg}$ is strongly correlated with silica content of the glass (after correcting for the effects of alkalis) and olivine Fo content. We therefore projected each $K_{D,Fe^{2+}-Mg}$ value calculated using one of the Fe^{3+}/Fe^{2+} algorithms to 'S' = 0·5, an arbitrary value close to the median 'S' = 0·48 for all of the glass compositions. Each set of projected $K_{D,Fe^{2+}-Mg}$ values was then fitted to a linear function in Fo content and projected to an olivine composition of Fo_{88} (the Supplementary Material provides a detailed description of the projection scheme). We emphasize that our goal is not to provide a formal parameterization of $K_{D,Fe^{2+}-Mg}$, but to minimize the compositional effects on $K_{D,Fe^{2+}-Mg}$ so as to compare the effect of different Fe^{3+}/Fe^{2+} calculation schemes using as large a population of olivine–liquid pairs as possible.

The projection procedure described above and in the Supplementary Material removes the effect of olivine composition on $K_{D,Fe^{2+}-Mg}$ and substantially reduces the effects of silica and total alkalis. Two of the projected datasets, those calculated using Borisov & Shapkin (1989) and Jayasuriya *et al.* (2004) equation (14), show a weak but statistically significant correlation with weight per cent SiO_2 (r_S is equal to −0·12 and −0·13, respectively) and all of the projected datasets are weakly correlated with weight per cent $Na_2O + K_2O$ (r_S lies between −0·30 and −0·18). Linear fits of the projected $K_{D,Fe^{2+}-Mg}$ values as a function of weight per cent $Na_2O + K_2O$ yield, however, slopes that are ≤0·0014 (≤0·0008 for five of the seven sets), an order of magnitude lower than for the unprojected $K_{D,Fe^{2+}-Mg}$ values. Figure 4 shows histograms of the projected $K_{D,Fe^{2+}-Mg}$ values based on five of the eight Fe^{3+}/Fe^{2+} calculation schemes. Mean absolute deviations, which we use as an indication of the width of a distribution, are all in the range of 0·014–0·015, and, with the

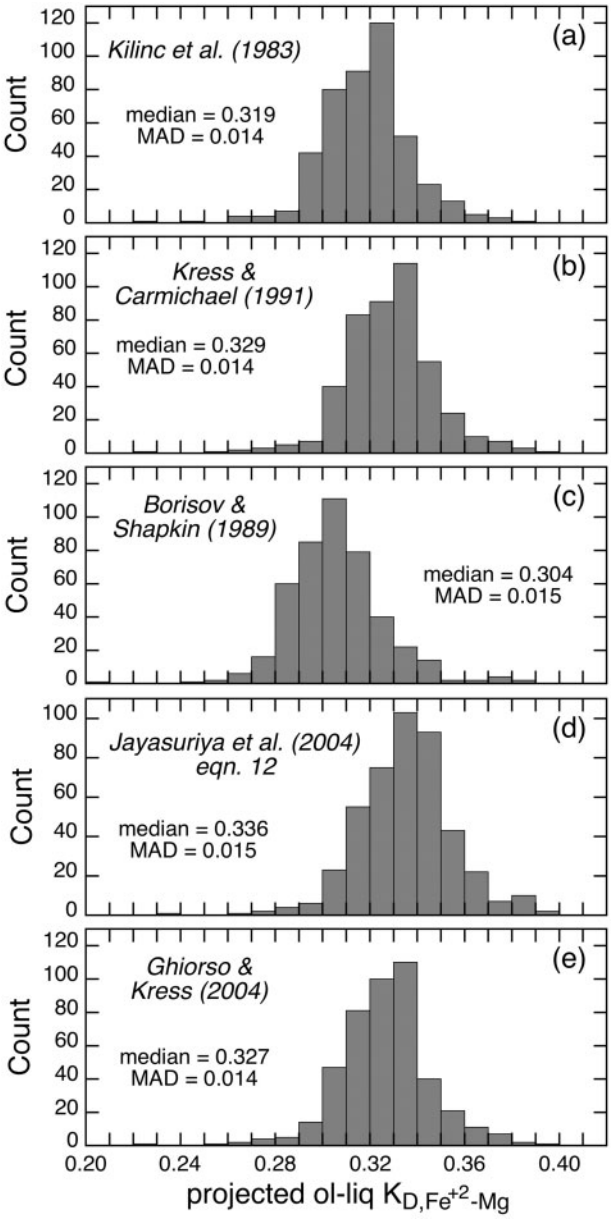

Fig. 4. Histograms of projected olivine–liquid $K_{D,Fe^{2+}-Mg}$ values for QFM ± 0·25 experiments from the literature (see Supplementary Material at http://www.petrology.oxfordjournals.org/ for references) based on quenched liquid FeO contents calculated using Fe^{3+}/Fe^{2+} algorithms of: (a) Kilinc *et al.* (1983), (b) Kress & Carmichael (1991), (c) Borisov & Shapkin (1989), (d) equation (12) of Jayasuriya *et al.* (2004), and (e) Ghiorso & Kress (2004). Median values and mean absolute deviations (based on the median value) are given for each panel. The projection scheme, which removes much (but not all) of the effects of liquid and olivine composition on $K_{D,Fe^{2+}-Mg}$, is described in the text and in more detail in the Supplementary Material.

exception of $K_{D,Fe^{2+}-Mg}$ values calculated using Borisov & Shapkin (1989), the median values all overlap at 1 MAD; the algorithms of Jayasuriya *et al.* (2004) yield the highest median $K_{D,Fe^{2+}-Mg}$ values [0·336, equation (12), Fig. 4d and 0·330, equation (14), not shown] and those of Borisov & Shapkin (1989) yield the lowest (0·304). We applied the same projection procedure to the $\leq IW + 0{\cdot}5$ dataset as we did for $QFM \pm 0{\cdot}25$. All median projected $K_{D,Fe^{2+}-Mg}$ values lie between 0·332 and 0·337 and, with the exception of those of Borisov & Shapkin (1989), all of them overlap at 1 MAD. We selected equation (12) of Jayasuriya *et al.* (2004) for calculating Fe^{3+}/Fe^{2+} in Hawaiian parental liquids because it has the smallest difference between median projected $K_{D,Fe^{2+}-Mg}$ values for the $\leq IW + 0{\cdot}5$ and $QFM \pm 0{\cdot}25$ datasets. It is, however, important to stress that we lack sufficient data to determine which Fe^{3+}/Fe^{2+} model is the most accurate (many more Fe^{3+}/Fe^{2+} measurements are needed, especially under conditions more oxidizing than QFM). That said, self-consistency across ranges of redox conditions is important in any model and this leads us to favor equation (12) of Jayasuriya *et al.* (2004).

We noted above (e.g. Fig. 3) that, under highly oxidizing conditions, there is a discrepancy between $K_{D,Fe^{2+}-Mg}$ values for run 39 in which Fe^{3+}/Fe^{2+} was measured and for which Fe^{3+}/Fe^{2+} was calculated. Figure 5 shows projected $K_{D,Fe^{2+}-Mg}$ values (thus removing most of the liquid and olivine compositional dependences on $K_{D,Fe^{2+}-Mg}$) as a function of the deviation in $\log fO_2$ from QFM. Median projected $K_{D,Fe^{2+}-Mg}$ values calculated using equation (12) of Jayasuriya *et al.* (2004; black symbols) and those for which Fe^{3+}/Fe^{2+} was measured, either by Mössbauer spectroscopy (open circles) or wet chemistry (gray circles), overlap for fO_2 values $\leq \sim$QFM and are essentially constant. The Mössbauer spectroscopy and wet chemistry determinations are important because they are independent of Fe^{3+}/Fe^{2+} calculation schemes and they suggest that, for the redox conditions most relevant to terrestrial and planetary basalts, Fe^{3+} in the liquid does not significantly affect the solution properties of MgO and FeO in the melt and, therefore, the value of $K_{D,Fe^{2+}-Mg}$. As the fO_2 is increased above these low levels, however, median projected $K_{D,Fe^{2+}-Mg}$ values increasingly diverge from the $\sim$0·34 characteristic of more reducing conditions. This may reflect the influence of Fe^{3+} on the thermodynamic properties of basaltic liquids and definitely implies that the application of constant $K_{D,Fe^{2+}-Mg}$ values to highly oxidizing systems should be approached with caution.

Projected $K_{D,Fe^{2+}-Mg}$ values can be used to compare Fe^{3+}/Fe^{2+} algorithms and the possible influence of Fe^{3+} on $K_{D,Fe^{2+}-Mg}$, as discussed above. It is, however, also important to establish the temperature–fO_2 and compositional bounds over which a single unprojected value of $K_{D,Fe^{2+}-Mg}$ can be assumed, as this greatly simplifies

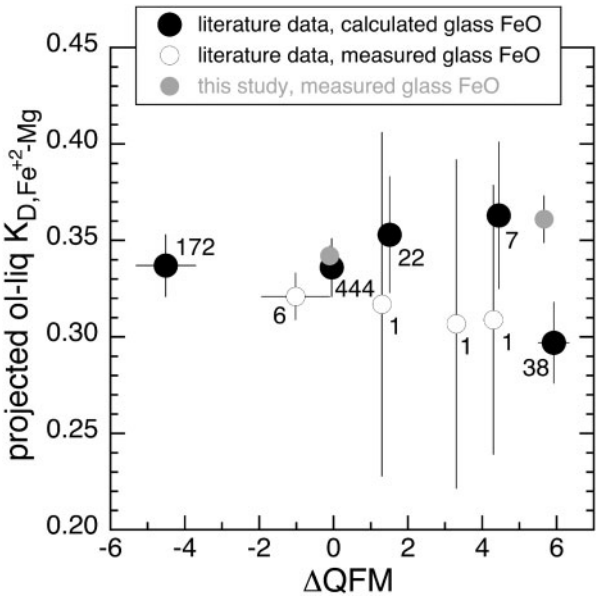

Fig. 5. Median and single projected $K_{D,Fe^{2+}-Mg}$ values as a function of the deviation in $\log fO_2$ from QFM (O'Neill, 1987); projection methods are described in the text and in more detail in the Supplementary Material. Filled black circles are median values for literature data based on equation (12) of Jayasuriya *et al.* (2004); data were binned in groups with $\log fO_2$ in the range of $\leq IW + 0{\cdot}5$, $QFM \pm 0{\cdot}25$, $QFM + 1{\cdot}5 \pm 0{\cdot}5$, $QFM + 4{\cdot}5 \pm 0{\cdot}5$, and air. Open circles are from literature experiments with measured FeO contents; filled gray circles are the QFM and air experiments from this study (Table 3). Numbers adjacent to symbols are the number of experiments represented by the point; if >1, then the plotted values are medians, the *y*-axis error bars represent mean absolute deviations, and the *x*-axis error bars are 1 standard deviation with respect to ΔQFM, the deviation in $\log fO_2$ from the QFM buffer at the same temperature. For the three open circles that represent a single $K_{D,Fe^{2+}-Mg}$ value (Mysen 2006), and the two filled-gray circles (this study), the *y*-axis errors represent uncertainties on the $K_{D,Fe^{2+}-Mg}$ values obtained from propagating the 1σ uncertainties associated with the FeO and MgO contents of the quenched melts and olivines. The unusually large error bars associated with the three open circles reflect the uncertainties associated with the MgO and FeO contents of the olivines in the experiments of Mysen (2006). References for the other literature data are given in the Supplementary Material.

modeling olivine fractionation in natural systems. A variety of constant $K_{D,Fe^{2+}-Mg}$ values have been offered, sometimes tailored to specific magmatic systems (e.g. Roeder & Emslie, 1970; Nisbet *et al.*, 1987; Putirka *et al.*, 2007), but none of these are applicable to all liquid and olivine compositions. Let us consider, for example, the variation of $K_{D,Fe^{2+}-Mg}$ with alkalis in the liquid (Fig. 6). For low $Na_2O + K_2O$ (e.g. <3 wt %), $K_{D,Fe^{2+}-Mg}$ can be regarded as independent of alkali content but, as $Na_2O + K_2O$ is increased above a few weight per cent, $K_{D,Fe^{2+}-Mg}$ decreases markedly. Thus, modeling of olivine fractionation for magmas ranging from alkali-poor to alkali-rich would need to account for variations in $K_{D,Fe^{2+}-Mg}$ with changing alkali concentrations in the melt. The effect of alkalis on $K_{D,Fe^{2+}-Mg}$ can, however, be ignored for relatively

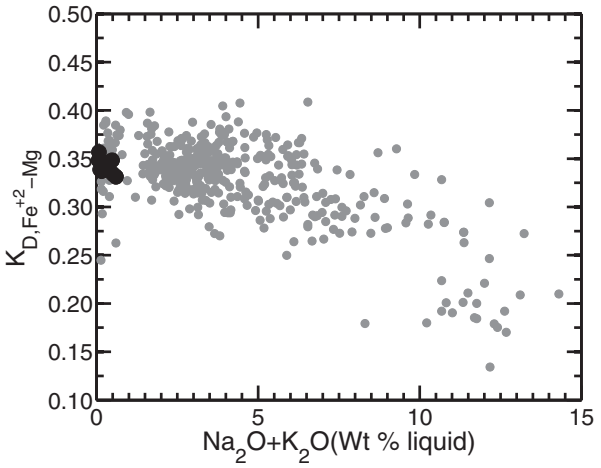

Fig. 6. $K_{D,Fe^{2+}-Mg}$ as a function of $Na_2O + K_2O$ (wt %) for QFM ± 0·25 data from this study (filled black circles) and literature data (filled gray circles) based on equation (12) of Jayasuriya *et al.* (2004). References for the literature data are given in the Supplementary Material.

low-alkali liquids. Similar arguments hold for silica. Low-silica melts yield low values of $K_{D,Fe^{2+}-Mg}$, although some of this may be an alkali effect (many silica-poor melts are also alkali-rich). Restricting melt compositions to 46–52 wt % SiO_2 and ≤3 wt % $Na_2O + K_2O$ avoids $K_{D,Fe^{2+}-Mg}$ values that vary strongly with liquid composition but still includes a range of natural basaltic to picritic liquids. The median $K_{D,Fe^{2+}-Mg}$ (unprojected) for 337 experimental glasses equilibrated at fO_2 values ≤ QFM + 0·25 with 46–52 wt % SiO_2 and ≤3 wt % $Na_2O + K_2O$, including those of the present study, is 0·343 ± 0·017 (MAD); the range in temperature and Fo content for these experiments is 1009–1571 °C and 36–95, respectively. $K_{D,Fe^{2+}-Mg}$ is weakly correlated with temperature ($r_s = -0·12$) and the SiO_2 content of the glass ($r_s = 0·12$), but for silica contents and temperatures for olivine crystallization from basaltic to picritic melts (46–52 wt % SiO_2; 1150–1500°C), these dependences have little effect (<0·013). $K_{D,Fe^{2+}-Mg}$ is negatively correlated with the Fo content of the olivine but for experiments with $Fo_{80–92}$ olivines, a range encompassing ~96% of over 17 000 olivine phenocryst analyses from the global dataset of Sobolev *et al.* (2007), the median $K_{D,Fe^{2+}-Mg}$ decreases only from 0·343 ± 0·017 to 0·337 ± 0·014 (144 experiments). We conclude that for relatively low-alkali terrestrial basalts, a constant $K_{D,Fe^{2+}-Mg}$ of 0·34 is adequate for simple petrological modeling and we use this value below in constructing estimates of Hawaiian parental magmas.

Hawaiian parental liquids

The compositions and characteristics of mantle sources and liquids in shallow pre-eruptive magma chambers are critical to understanding the nature and origin of Hawaiian lavas (e.g. Maaløe, 1979; Wright, 1984; Herzberg & O'Hara, 2002). Trace element and isotopic data have been used to address these issues (e.g. Hofmann & Jochum, 1996; Blichert-Toft *et al.*, 2003), as has the major element chemistry (e.g. Stolper *et al.*, 2004; Herzberg, 2006). For the major elements, different reconstruction approaches and model constraints have led to a range of inferred MgO contents in the parental or primary magmas (13–22 wt %; Wright, 1984; Clague *et al.*, 1991; Garcia *et al.*, 1995; Baker *et al.*, 1996; Rhodes, 1996; Norman & Garcia, 1999; Green *et al.*, 2001; Herzberg & O'Hara, 2002; Rhodes & Vollinger, 2004; Stolper *et al.*, 2004; Herzberg, 2006; Herzberg *et al.*, 2007; Putirka, 2008*a*). This range of estimates of the MgO contents of Hawaiian parental or primary magmas has attracted some attention because it has considerable petrogenetic significance (e.g. in the depth of separation of liquids from peridotitic residual sources and in estimates of mantle potential temperatures; Herzberg & O'Hara, 2002; Falloon *et al.*, 2007; Putirka *et al.*, 2007).

The usual approach to these types of parental liquid calculations [but see Norman & Garcia (1999) for an alternative] is to posit the composition of a target olivine, define Fe^{3+}/Fe^{2+} in the liquid either by specifying Fe^{3+}/Fe^{2+} or choosing the redox conditions and an algorithm to compute Fe^{3+}/Fe^{2+}, choose a single (unprojected) value of $K_{D,Fe^{2+}-Mg}$ to connect liquid and olivine compositions, and select a glass or aphyric lava whose composition is thought to be related through olivine fractionation to the parental melt. The fractionation process is then reversed numerically by dissolving small increments of equilibrium olivine back into the selected glass or aphyric lava until the resulting liquid is in equilibrium with the assumed composition of the target olivine. In this section, we first consider input parameters for parental melt calculations applicable to Mauna Loa, Mauna Kea and Kilauea, and then evaluate parental magmas for these three Hawaiian volcanoes using our constraints on $K_{D,Fe^{2+}-Mg}$.

Plausible target olivines for reversed fractionation calculations are usually either mantle phases postulated to be in equilibrium with the primary melt or the most Mg-rich olivine phenocryst found in lavas from the volcano in question (for a parental liquid). We chose the latter approach and have ignored the possible effects of pressure on Fe^{3+}/Fe^{2+} in the liquid and on $K_{D,Fe^{2+}-Mg}$; the assumption that olivine fractionation occurs primarily at low pressures is justified by fluid inclusions in olivine phenocrysts from Hawaiian lavas that suggest low formation pressures in the 2–5 kbar range (Roedder, 1983) and gravity anomalies associated with the summits and rift zones of all of the volcanoes on the Big Island (Kauahikaua *et al.*, 2000) that suggest substantial olivine fractionation occurs at relatively low pressures (~2 kbar). Under these conditions, the effect of pressure on Fe^{3+}/Fe^{2+} and $K_{D,Fe^{2+}-Mg}$ is believed to be modest (Toplis, 2005;

O'Neill *et al.*, 2006). Based on a large sample of olivine phenocryst compositions (Clague *et al.*, 1995; Garcia *et al.*, 1995; Baker *et al.*, 1996; Garcia, 1996; Sobolev *et al.*, 2007; D. A. Clague, unpublished data), the most magnesian olivines are $Fo_{90·8}$ for Kilauea, $Fo_{91·0}$ for Mauna Kea and $Fo_{91·7}$ for Mauna Loa.

Recent estimates of redox conditions for Hawaiian magmas based on Fe_2O_3/FeO determinations of glasses and aphyric lavas are generally in the vicinity of QFM − 1 (see Rhodes & Vollinger, 2005, and references therein). Bulk Fe_2O_3/FeO measured on near-vent aphyric Mauna Loa lavas yield fO_2 values of ~QFM − 2 (Rhodes & Vollinger, 2005); Cr-in-glass and FeO/Fe_2O_3 wet chemical measurements on near-vent, rapidly quenched Kilauea Pu'u 'O'o lavas yield values that range from ~QFM − 0·4 to QFM − 1·7 (Roeder *et al.*, 2003). Poustovetov & Roeder (2001) studied the partitioning of Cr between melt and spinel in a Kilauea basalt and obtained ~QFM − 0·5. Similar measurements are not available for Mauna Kea, so we accepted the range of estimates for Mauna Loa and Kilauea, QFM − 0·5 to QFM − 2, as bounding the redox conditions during low-pressure fractionation of olivine in the shield-building tholeiitic phases of this volcano.

Below ~7 wt % MgO, Hawaiian tholeiitic liquids become saturated with plagioclase and/or augite (Montierth *et al.*, 1995; Thornber *et al.*, 2003; Seaman *et al.*, 2004), so we restricted consideration to glasses with ≥7 wt % MgO; Supplementary Data Table A2 lists average glass compositions for Mauna Kea, Mauna Loa, and Kilauea volcanoes. All three of these compositions and their calculated parental liquids, as described below, are within the compositional bounds over which $K_{D,Fe^{2+}-Mg}$ can assumed to be constant based on our analysis given above. We compare reconstructed parental magma compositions for two constant values of $K_{D,Fe^{2+}-Mg}$: 0·34, the value most consistent with both our experimental data and the literature data (46–52 wt % SiO_2, ≤3 wt % $Na_2O + K_2O$) under relevant redox conditions (i.e. ≤ QFM + 0·25); and 0·30, the canonical value of Roeder & Emslie (1970).

Results of the parental melt calculations are shown in Fig. 7. Figure 7a shows the results of olivine-addition calculations (given in Table A3 in the Supplementary Material) for the 'low-SiO_2' glass composition of Mauna Kea (Table A2). Here, we explore the effects of varying the fO_2 (QFM − 0·5 to QFM − 2), the target olivine composition ($Fo_{90–91}$), and $K_{D,Fe^{2+}-Mg}$ (0·30–0·34) on the resulting parental liquid composition. The MgO contents of the calculated parental liquids vary from 15·5 (QFM − 0·5, Fo_{90}, $K_{D,Fe^{2+}-Mg} = 0·30$) to 21·4 wt % (QFM − 2, Fo_{91}, $K_{D,Fe^{2+}-Mg} = 0·34$), nearly spanning the range of estimated primary or parental Hawaiian magmas from the literature (see Fig. 7b; filled gray circles). Over these ranges in composition and fO_2, the calculated parental liquid compositions decrease by ~1 wt % MgO for every log unit increase in the selected fO_2 (from QFM − 2 to QFM − 0·5), for every 0·5 decrease in the forsterite content of the residual olivine (from Fo_{91} to Fo_{90}), and every 0·015 decrease in $K_{D,Fe^{2+}-Mg}$ (0·34–0·30). An important conclusion from these calculations is that, while holding △QFM and the forsterite content of residual olivine constant, a change in $K_{D,Fe^{2+}-Mg}$ from 0·30 to 0·34 leads to an ~2·6 wt % increase in the MgO content of the reconstructed parental liquid.

The results of olivine-addition calculations with Mauna Loa and Kilauea glasses and Mauna Kea low- and high-SiO_2 glass compositions (Table A3) are shown in Fig. 7b. Here we used $K_{D,Fe^{2+}-Mg}$ of 0·34 and △QFM values calculated from measured Fe_2O_3/FeO ratios in Mauna Loa and Kilauea lavas (and in the case of Kilauea, the Cr contents of these near-vent glasses); for Mauna Kea we assumed an fO_2 of QFM − 1, a conservative value consistent with estimates on Mauna Loa and Kilauea lavas (see Rhodes & Vollinger, 2005). Target olivine compositions (i.e. the endpoint of each olivine-addition calculation) were $Fo_{90·8}$ (Kilauea), $Fo_{91·7}$ (Mauna Loa), and $Fo_{91·0}$ (Mauna Kea). Calculated MgO contents for the parental Kilauea composition range from 19·0 to 19·7 depending on whether the fO_2 is assumed to be QFM − 0·7 [from Cr measurements of Roeder *et al.* (2003)] or QFM − 1·4 (based on Fe_2O_3/FeO measurements; Roeder *et al.*, 2003). The calculated MgO content of the Mauna Loa parental composition is 21·2 wt %. For the low- and high-SiO_2 Mauna Kea glasses, calculated MgO contents are 20·5 and 19·0 wt %, respectively. For comparison, the filled gray circles in Fig. 7b show estimated MgO contents of parental or primary Hawaiian magmas from the literature (Wright, 1984; Clague *et al.*, 1991; Garcia *et al.*, 1995; Baker *et al.*, 1996; Rhodes, 1996; Green *et al.*, 2001; Herzberg & O'Hara, 2002; Rhodes & Vollinger, 2004; Stolper *et al.*, 2004; Herzberg, 2006; Herzberg *et al.*, 2007; Putirka, 2008*a*). For a given target olivine composition, relatively low MgO values generally reflect the use of a $K_{D,Fe^{2+}-Mg}$ of 0·30 and/or an fO_2 of ~QFM (or a fixed FeO/FeO* ratio of 0·9), whereas high MgO estimates reflect the use of a $K_{D,Fe^{2+}-Mg}$ of ~0·34 (e.g. Herzberg & O'Hara, 2002) or conditions more reducing than QFM (note that the initial FeO* content of the starting composition also influences the final MgO value). If Hawaiian tholeiitic magmas undergoing shallow-level fractionation are as reducing as the near-vent glass FeO contents seem to suggest, and if the rare >Fo_{90} olivines represent the earliest fractionation products of these magma, then it seems hard to avoid parental magma estimates with at least 18–19 wt % MgO. Such MgO-rich magmas have obvious implications for melting temperatures within the Hawaiian plume—a topic that is beyond the scope of this work—but one that has been addressed in a number of recent papers (e.g. Falloon *et al.*, 2007; Herzberg *et al.*, 2007; Putirka *et al.*, 2007).

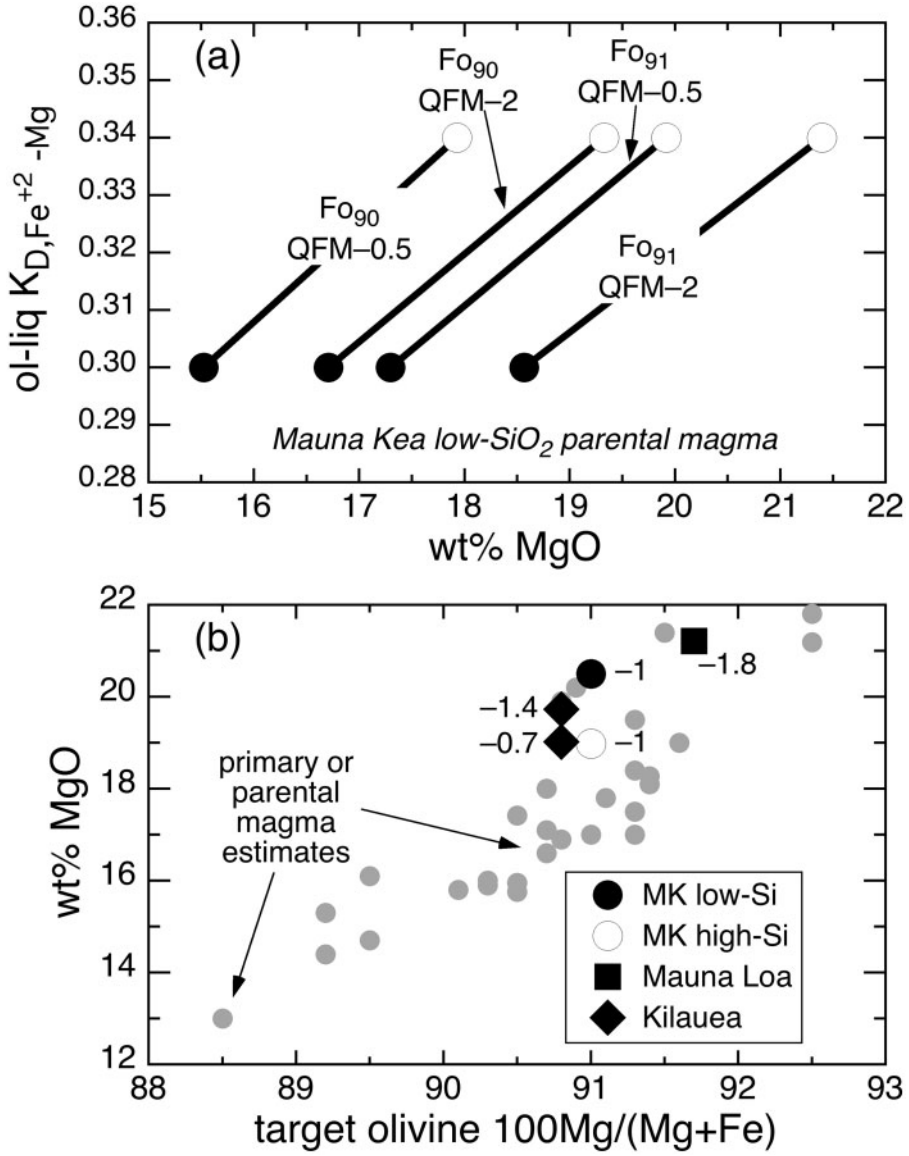

Fig. 7. (a) Ol–liq $K_{D,Fe^{2+}-Mg}$ vs MgO content (in wt %) of calculated parental magmas produced by near-fractional olivine addition to the mean composition of the undegassed 'low-SiO_2' glasses (see the Supplementary Material, Table A2) from the Mauna Kea portion of the HSDP2 core (Stolper *et al.*, 2004). The near-fractional olivine-addition calculation is described in the notes to Table A3 in the Supplementary Material; the fO_2 (relative to QFM; O'Neill, 1987) and the endpoint olivine composition are given for each pair of calculations (closed circles for $K_{D,Fe^{2+}-Mg} = 0{\cdot}30$; open circles for $K_{D,Fe^{2+}-Mg} = 0{\cdot}34$). Calculated compositions are reported in Table A3. (b) Estimated parental MgO contents for Mauna Loa, Kilauea, and Mauna Kea volcanoes (this study) as a function of target olivine $100 \times Mg/(Mg + Fe)$, atomic. Starting compositions are given in Table A2; calculated liquids are reported in Table A3. All calculations were carried out using $K_{D,Fe^{2+}-Mg} = 0{\cdot}34$ and various log fO_2 values relative to QFM (O'Neill, 1987), which are given next to symbols in the panel. Values of −1·8 (Mauna Loa) and −1·4 (Kilauea) represent median ΔQFM values based on Fe^{3+}/Fe^{2+} measurements of Rhodes & Vollinger (2005) and Roeder *et al.* (2003), respectively. The value of −0·7 for one of the Kilauea points is the median ΔQFM based on glass Cr contents (Roeder *et al.*, 2003) and the algorithm of Poustovetov & Roeder (2001). For the two Mauna Kea (MK) calculations, ΔQFM was assumed to be −1. The small filled gray circles are estimates of parental or primary Hawaiian magma compositions from Wright (1984), Clague *et al.* (1991), Garcia *et al.* (1995), Baker *et al.* (1996), Rhodes (1996), Green *et al.* (2001), Herzberg & O'Hara (2002), Rhodes & Vollinger (2004), Stolper *et al.* (2004), Herzberg (2006), Herzberg *et al.* (2007) and Putirka (2008*a*).

CONCLUSIONS

Our 1 atm experiments on a synthetic Hawaiian picrite composition (25·7 wt % MgO) yielded olivine–liquid pairs over a temperature range of ~1300–1500°C. For experiments conducted along the QFM buffer, olivine becomes progressively less forsteritic with decreasing temperature (i.e. from $Fo_{92{\cdot}3}$ to $Fo_{87{\cdot}3}$). With increasing fO_2 at constant temperature, the modal abundance of olivine in our experiments decreases and the olivine becomes

more forsteritic (e.g. at 1400°C, olivines are Fo_{90} at QFM and Fo_{97} in air), observations qualitatively consistent with MELTS calculations on the same bulk composition. MgO contents of the olivine-bearing glasses at QFM and NNO are approximately linear functions of temperature; an unweighted least-squares fit to our QFM data yields $T(^\circ C) = 19{\cdot}2 \times (\text{wt \% MgO in liquid}) + 1048$, which can be used as a semi-quantitative geothermometer for Hawaiian glass or whole-rock compositions with $>\sim 7$ wt % MgO.

The olivine–liquid Fe^{2+}–Mg exchange coefficient for our 11 experiments is $0{\cdot}345 \pm 0{\cdot}009$ (mean and 1σ, respectively), and is independent of temperature and liquid composition. The mean value from our QFM experiments, $0{\cdot}343 \pm 0{\cdot}008$, agrees well with the median value of $0{\cdot}340 \pm 0{\cdot}012$ (MAD) from 78 olivine–glass pairs from the literature with broadly tholeiitic compositions (46–52 wt % SiO_2, ≤ 3 wt % $Na_2O + K_2O$, and $Fo_{80–92}$) and run under similar fO_2 values (QFM $\pm$ 0·25). Within these bounds, olivine–liquid $K_{D,Fe^{2+}-Mg}$ values calculated using FeO contents in the liquid based on equation (12) of Jayasuriya *et al.* (2004) are approximately independent of composition and temperature.

Over the compositional range encompassed by Hawaiian tholeiitic lavas and their parental melts, $K_{D,Fe^{2+}-Mg}$ is $\sim 0{\cdot}34$ and, given the redox conditions and an Fo content for the most magnesian olivine phenocrysts, a parental melt composition can be predicted. The calculated compositions of the parental melts are sensitive to the input parameters, decreasing by ~ 1 wt % MgO for every log unit increase in the selected fO_2, every 0·5 decrease in the Fo content of the target olivine, and every 0·015 decrease in $K_{D,Fe^{2+}-Mg}$. For plausible ranges of redox conditions and Fo contents of the most MgO-rich olivine phenocrysts, the parental liquids for Hawaiian tholeiites must be highly magnesian, in the range of 19–21 wt % MgO for Kilauea, Mauna Loa, and Mauna Kea.

ACKNOWLEDGEMENTS

We thank Ma Chi for assistance with the analytical work on the electron microprobe and are especially appreciative of Rebecca Lange for providing FeO wet chemical measurements. The comments of S. Parman, K. Putirka, and M. Toplis led to significant improvements in the text and a more careful look at the seminal work of Roeder & Emslie. Finally, we would very much like to acknowledge Peter Roeder for the truly amazing feat of locating an unpublished data table four decades after it was produced and his willingness to share it.

FUNDING

This work was supported by National Science Foundation grant EAR-9528594, National Aeronautics and Space Administration grant NNX09AG40G, and a National Science Foundation GRF (AKM).

SUPPLEMENTARY DATA

Supplementary data for this paper are available at *Journal of Petrology* online.

REFERENCES

Agee, C. B. & Walker, D. (1990). Aluminum partitioning between olivine and ultrabasic silicate liquid to 6 GPa. *Contributions to Mineralogy and Petrology* **105**, 243–254.

Albarède, F. & Provost, A. (1977). Petrological and geochemical mass-balance equations: an algorithm for least-square fitting and general error analysis. *Computers and Geosciences* **3**, 309–326.

Armstrong, J. T. (1988). Quantitative analysis of silicate and oxide materials: comparison of Monte Carlo, ZAF and $\phi(\rho z)$ procedures. In: Newbury, D. E. (ed.) *Microbeam Analysis*. San Francisco, CA: San Francisco Press, pp. 239–246.

Baker, M. B., Alves, S. & Stolper, E. M. (1996). Petrography and petrology of the Hawaii Scientific Drilling Project lavas: Inferences from olivine phenocryst abundances and compositions. *Journal of Geophysical Research* **101**, 11715–11727.

Basaltic Volcanism Study Project. (1981). *Basaltic Volcanism on the Terrestrial Planets*. New York: Pergamon Press.

Beattie, P., Ford, C. & Russell, D. (1991). Partition coefficients for olivine–melt and orthopyroxene–melt systems. *Contributions to Mineralogy and Petrology* **109**, 212–224.

Beckett, J. R. & Mendybaev, R. A. (1997). The measurement of oxygen fugacities in flowing gas mixtures at temperatures below 1200°C. *Geochimica et Cosmochimica Acta* **61**, 4331–4336.

Bédard, J. H. (1994). A procedure for calculating the equilibrium distribution of trace elements among the minerals of cumulate rocks, and the concentration of trace elements in the coexisting liquids. *Chemical Geology* **118**, 143–153.

Bédard, J. H. (2005). Partitioning coefficients between olivine and silicate melts. *Lithos* **83**, 394–419.

Blichert-Toft, J., Weis, D., Maerschalk, C., Agranier, A. & Albarède, F. (2003). Hawaiian hot spot dynamics as inferred from the Hf and Pb isotope evolution of Mauna Kea volcano. *Geochemistry, Geophysics, Geosystems* **4**, 8704, doi:10.1029/2002GC000340.

Borisov, A. A. & Shapkin, A. I. (1989). New empirical equation rating Fe^{3+}/Fe^{2+} in magmas to their composition, oxygen fugacity, and temperature. *Geokhimiya*, **1989(6)**, 892–897 [*Geochemistry International* (1989) **27**(1), 111–116].

Carmichael, I. S. E. (1991). The redox states of basic and silicic magmas: a reflection of their source regions? *Contributions to Mineralogy and Petrology* **106**, 129–141.

Clague, D. A., Weber, W. S. & Dixon, J. E. (1991). Picritic glasses from Hawaii. *Nature* **353**, 553–556.

Clague, D. A., Moore, J. G., Dixon, J. E. & Friesen, W. B. (1995). Petrology of submarine lavas from Kilauea's Puna Ridge, Hawaii. *Journal of Petrology* **36**, 299–349.

Corrigan, G. & Gibb, F. G. F. (1979). The loss of Fe and Na from a basaltic melt during experiments using the wire-loop method. *Mineralogical Magazine* **43**, 121–126.

Cottrell, E., Kelley, K. A., Lanzirotti, A. & Fischer, R. A. (2009). High-precision determination of iron oxidation state in silicate glasses using XANES. *Chemical Geology* **268**, 167–179.

Drake, M. J. & Holloway, J. R. (1981). Partitioning of Ni between olivine and silicate melt: the 'Henry's Law problem' reexamined. *Geochimica et Cosmochimica Acta* **45**, 431–437.

Eggins, S. M. (1992). Petrogenesis of Hawaiian tholeiites: 1, phase equilibria constraints. *Contributions to Mineralogy and Petrology* **110**, 387–397.

Eugster, H. P. & Wones, D. R. (1962). Stability relations of the ferruginous biotite, annite. *Journal of Petrology* **3**, 82–125.

Falloon, T. J., Danyushevsky, L. V., Ariskin, A., Green, D. H. & Ford, C. E. (2007). The application of olivine geothermometry to infer crystallization temperatures of parental liquids: Implications for the temperature of MORB magmas. *Chemical Geology* **241**, 207–233.

Ford, C. E., Russell, D. G., Craven, J. A. & Fisk, M. R. (1983). Olivine–liquid equilibria: Temperature, pressure and composition dependence of the crystal/liquid cation partition coefficients for Mg, Fe^{2+}, Ca and Mn. *Journal of Petrology* **24**, 256–265.

Garcia, M. O. (1996). Petrography and olivine and glass chemistry of lavas from the Hawaii Scientific Drilling Project. *Journal of Geophysical Research* **101**, 11701–11713.

Garcia, M. O., Hulsebosch, T. P. & Rhodes, J. M. (1995). Olivine-rich submarine basalts from the southwest rift zone of Mauna Loa Volcano: implications for magmatic processes and geochemical evolution. In: Rhodes, J. M. & Lockwood, J. P. (eds) *Mauna Loa Revealed: Structure, Composition, History, and Hazards. Geophysical Monograph, American Geophysical Union* **92**, 219–239.

Gee, L. L. & Sack, R. O. (1988). Experimental petrology of melilite nephelinites. *Journal of Petrology* **29**, 1233–1255.

Ghiorso, M. S. & Kress, V. C. (2004). An equation of state for silicate melts. II. Calibration of volumetric properties at 10^5 Pa. *American Journal of Science* **304**, 679–751.

Ghiorso, M. S. & Sack, R. O. (1995). Chemical mass transfer in magmatic processes IV. A revised and internally consistent thermodynamic model for the interpolation and extrapolation of liquid–solid equilibria in magmatic systems at elevated temperatures and pressures. *Contributions to Mineralogy and Petrology* **119**, 197–212.

Goldberg, R. N. & Weir, R. D. (1992). Conversion of temperatures and thermodynamic properties to the basis of the international temperature scale of 1990. *Pure and Applied Chemistry* **64**, 1545–1562.

Green, D. H., Falloon, T. J., Eggins, S. M. & Yaxley, G. M. (2001). Primary magmas and mantle temperatures. *European Journal of Mineralogy* **13**, 437–451.

Grove, T. L. (1981). Use of FePt alloys to eliminate the iron loss problem in 1 atmosphere gas mixing experiments: Theoretical and practical considerations. *Contributions to Mineralogy and Petrology* **78**, 298–304.

Grove, T. L., Kinzler, R. J. & Bryan, W. B. (1992). Fractionation of mid-ocean ridge basalt (MORB). In: Morgan, J. P., Blackman, D. K. & Sinton, J. M. (eds) *Mantle Flow and Melt Generation at Mid-Ocean Ridges. Geophysical Monograph, American Geophysical Union* **71**, 281–310.

Hanson, B. & Jones, J. H. (1998). The systematics of Cr^{+3} and Cr^{+2} partitioning between olivine and liquid in the presence of spinel. *American Mineralogist* **83**, 669–684.

Hart, S. R. & Davis, K. E. (1978). Nickel partitioning between olivine and silicate melt. *Earth and Planetary Science Letters* **40**, 203–219.

Helz, R. T. & Thornber, C. R. (1987). Geothermometry of Kilauea Iki lava lake, Hawaii. *Bulletin of Volcanology* **49**, 651–668.

Herzberg, C. (2006). Petrology and thermal structure of the Hawaiian plume from Mauna Kea volcano. *Nature* **444**, 605–609.

Herzberg, C. & O'Hara, M. J. (2002). Plume-associated ultramafic magmas of Phanerozoic age. *Journal of Petrology* **43**, 1857–1883.

Herzberg, C., Asimow, P. D., Arndt, N., Niu, Y., Lesher, C. M., Fitton, J. G., Cheadle, M. J. & Saunders, A. D. (2007). Temperatures in ambient mantle and plumes: Constraints from basalts, picrites, and komatiites. *Geochemistry, Geophysics, Geosystems* **8**, Q02006, doi:10.1029/2006GC001390.

Hill, R. & Roeder, P. (1974). The crystallization of spinel from basaltic liquid as a function of oxygen fugacity. *Journal of Geology* **82**, 709–729.

Hirschmann, M. M. & Ghiorso, M. S. (1994). Activities of nickel, cobalt, and manganese silicates in magmatic liquids and applications to olivine/liquid and to silicate/metal partitioning. *Geochimica et Cosmochimica Acta* **58**, 4109–4126.

Hirschmann, M. M., Ghiorso, M. S., Davis, F. A., Gordon, S. M., Mukherjee, S., Grove, T. L., Krawczynski, M., Medard, E. & Till, C. B. (2008). Library of experimental phase relations (LEPR): a database and web portal for experimental magmatic phase equilibria data. *Geochemistry, Geophysics, Geosystems* **9**, Q03011, doi:10.1029/2007GC001894.

Hofmann, A. W. & Jochum, K. P. (1996). Source characteristics derived from very incompatible trace elements in Mauna Loa and Mauna Kea basalts, Hawaii Scientific Drilling Project. *Journal of Geophysical Research* **101**, 11831–11839.

Huebner, J. S. (1971). Buffering techniques for hydrostatic systems at elevated pressures. In: Ulmer, G. C. (ed.) *Research Techniques for High Pressure and High Temperature*. New York: Springer, pp. 123–177.

Jayasuriya, K. D., O'Neill, H. St. C., Berry, A. J. & Campbell, S. J. (2004). A Mössbauer study of the oxidation state of Fe in silicate melts. *American Mineralogist* **89**, 1597–1609.

Kamenetsky, V. S., Crawford, A. J. & Meffre, S. (2001). Factors controlling chemistry of magmatic spinel: an empirical study of associated olivine, Cr-spinel and melt inclusions from primitive rocks. *Journal of Petrology* **42**, 655–671.

Kauahikaua, J., Hildenbrand, T. & Webring, M. (2000). Deep magmatic structures of Hawaiian volcanoes, imaged by three-dimensional gravity models. *Geology* **28**, 883–886.

Kilinc, A., Carmichael, I. S. E., Rivers, M. L. & Sack, R. O. (1983). The ferric–ferrous ratio of natural silicate liquids equilibrated in air. *Contributions to Mineralogy and Petrology* **83**, 136–140.

Kress, V. C. & Carmichael, I. S. E. (1988). Stoichiometry of the iron oxidation reaction in silicate melts. *American Mineralogist* **73**, 1267–1274.

Kress, V. C. & Carmichael, I. S. E. (1991). The compressibility of silicate liquids containing Fe_2O_3 and the effect of composition, temperature, oxygen fugacity and pressure on their redox states. *Contributions to Mineralogy and Petrology* **108**, 82–92.

Kushiro, I. & Mysen, B. O. (2002). A possible effect of melt structure on the Mg–Fe^{2+} partitioning between olivine and melt. *Geochimica et Cosmochimica Acta* **66**, 2267–2272.

Kushiro, I. & Walter, M. J. (1998). Mg–Fe partitioning between olivine and mafic–ultramafic melts. *Geophysical Research Letters* **25**, 2337–2340.

Le Maitre, R. W. (1976). The chemical variability of some common igneous rocks. *Journal of Petrology* **17**, 589–637.

Libourel, G. (1999). Systematics of calcium partitioning between olivine and silicate melt: implications for melt structure and calcium content of magmatic olivines. *Contributions to Mineralogy and Petrology* **136**, 63–80.

Longhi, J. (1982). Effects of fractional crystallization and cumulus processes on mineral composition trends of some lunar and terrestrial rock series. *Proceedings of the 13th Lunar and Planetary Science Conference, Part 1. Journal of Geophysical Research* **87**, Supplement, A54–A64.

Longhi, J., Walker, D. & Hays, J. F. (1978). The distribution of Fe and Mg between olivine and lunar basaltic liquids. *Geochimica et Cosmochimica Acta* **42**, 1545–1558.

Maaløe, S. (1979). Compositional range of primary tholeiitic magmas evaluated from major-element trends. *Lithos* **12**, 59–72.

Macdonald, G. A. & Katsura, T. (1964). Chemical composition of Hawaiian lavas. *Journal of Petrology* **5**, 82–133.

Mäkipää, H. T. (1980). Partitioning of chromium, manganese, cobalt and nickel between olivine and basaltic liquid; an experimental study. *Bulletin of the Geological Society of Finland* **52**, 175–191.

Mallmann, G. & O'Neill, H. St. C. (2009). The crystal/melt partitioning of V during mantle melting as a function of oxygen fugacity compared with some other elements (Al, P, Ca, Sc, Ti, Cr, Fe, Ga, Y, Zr and Nb). *Journal of Petrology* **50**, 1765–1794.

Médard, E., McCammon, C. A., Barr, J. A. & Grove, T. L. (2008). Oxygen fugacity, temperature reproducibility, and H_2O contents of nominally anhydrous piston-cylinder experiments using graphite capsules. *American Mineralogist* **93**, 1838–1844.

Montierth, C., Johnston, A. D. & Cashman, K. V. (1995). An empirical glass-composition-based geothermometer for Mauna Loa lavas. In: Rhodes, J. M. & Lockwood, J. P. (eds) *Mauna Loa Revealed: Structure, Composition, History, and Hazards. Geophysical Monograph, American Geophysical Union* **92**, 207–217.

Muan, A. & Osborn, E. F. (1956). Phase equilibria at liquidus temperatures in the system MgO–FeO–Fe_2O_3–SiO_2. *Journal of the American Ceramic Society* **39**, 121–140.

Murck, B. W. & Campbell, I. H. (1986). The effects of temperature, oxygen fugacity and melt composition on the behaviour of chromium in basic and ultrabasic melts. *Geochimica et Cosmochimica Acta* **50**, 1871–1887.

Mysen, B. O. (2006). Redox equilibria of iron and silicate melt structure: Implications for olivine/melt element partitioning. *Geochimica et Cosmochimica Acta* **70**, 3121–3138.

Mysen, B. (2007). Partitioning of calcium, magnesium, and transition metals between olivine and melt governed by the structure of the silicate melt at ambient pressure. *American Mineralogist* **92**, 844–862.

Mysen, B. O. & Dubinsky, E. V. (2004). Melt structural control on olivine/melt element partitioning of Ca and Mn. *Geochimica et Cosmochimica Acta* **68**, 1617–1633.

Mysen, B. O. & Shang, J. (2005). Evidence from olivine/melt element partitioning that nonbridging oxygen in silicate melts are not equivalent. *Geochimica et Cosmochimica Acta* **69**, 2861–2875.

Nielsen, R. L. & DeLong, S. E. (1992). A numerical approach to boundary layer fractionation: application to differentiation in natural magma systems. *Contributions to Mineralogy and Petrology* **110**, 355–369.

Nisbet, E. G., Arndt, N. T., Bickle, M. J., Cameron, W. E., Chauvel, C., Cheadle, M., Hegner, E., Kyser, T. K., Martin, A., Renner, R. & Roedder, E. (1987). Uniquely fresh 2·7 Ga komatiites from the Belingwe greenstone belt, Zimbabwe. *Geology* **15**, 1147–1150.

Norman, M. D. & Garcia, M. O. (1999). Primitive magmas and source characteristics of the Hawaiian plume: petrology and geochemistry of shield picrites. *Earth and Planetary Science Letters* **168**, 27–34.

O'Neill, H. St. C. (1987). Quartz–fayalite–iron and quartz–fayalite–magnetite equilibria and the free energy of formation of fayalite (Fe_2SiO_4) and magnetite (Fe_3O_4). *American Mineralogist* **72**, 67–75.

O'Neill, H. St. C., Berry, A. J., McCammon, C. C., Jayasuriya, K. D., Campbell, S. J. & Foran, G. (2006). An experimental determination of the effect of pressure on the $Fe^{3+}/\Sigma Fe$ ratio of an anhydrous silicate melt to 3·0 GPa. *American Mineralogist* **91**, 404–412.

Parman, S. W., Dann, J. C., Grove, T. L. & deWit, M. J. (1997). Emplacement conditions of komatiite magmas from the 3·49 Ga Komati Formation, Barberton Greenstone Belt, South Africa. *Earth and Planetary Science Letters* **150**, 303–323.

Partzsch, G. M., Lattard, D. & McCammon, C. (2004). Mössbauer spectroscopic determination of Fe^{3+}/Fe^{2+} in synthetic basaltic glass: a test of empirical fO_2 equations under superliquidus and subliquidus conditions. *Contributions to Mineralogy and Petrology* **147**, 565–580.

Poustovetov, A. A. & Roeder, P. L. (2001). The distribution of Cr between basaltic melt and chromian spinel as an oxygen geobarometer. *Canadian Mineralogist* **39**, 309–317.

Powers, H. A. (1955). Composition and origin of basaltic magma of the Hawaiian Islands. *Geochimica et Cosmochimica Acta* **7**, 77–107.

Press, W. H., Teukolsky, S. A., Vetterling, W. T. & Flannery, B. P. (1992). *Numerical Recipes*, 2nd edn. Cambridge: Cambridge University Press.

Putirka, K. (2008*a*). Excess temperatures at ocean islands: Implications for mantle layering and convection. *Geology* **36**, 283–286.

Putirka, K. (2008*b*). Thermometers and barometers for volcanic systems. In: Putirka, K. D. & Tepley, F. J., III (eds) *Minerals, Inclusions and Volcanic Processes. Mineralogical Society of America and Geochemical Society, Reviews in Mineralogy and Geochemistry* **69**, 61–120.

Putirka, K. D., Perfit, M., Ryerson, F. J. & Jackson, M. G. (2007). Ambient and excess mantle temperatures, olivine thermometry, and active vs passive upwelling. *Chemical Geology* **241**, 177–206.

Rhodes, J. M. (1996). Geochemical stratigraphy of lava flows sampled by the Hawaii Scientific Drilling Project. *Journal of Geophysical Research* **101**, 11729–11746.

Rhodes, J. M. & Vollinger, M. J. (2004). Composition of basaltic lavas sampled by phase-2 of the Hawaii Scientific Drilling Project: Geochemical stratigraphy and magma types. *Geochemistry, Geophysics, Geosystems* **5**, Q03G13, doi:10.1029/2002GC000434.

Rhodes, J. M. & Vollinger, M. J. (2005). Ferric/ferrous ratios in 1984 Mauna Loa lavas: a contribution to understanding the oxidation state of Hawaiian magmas. *Contributions to Mineralogy and Petrology* **149**, 666–674.

Righter, K., Drake, M. J. & Yaxley, G. (1997). Prediction of siderophile element metal-silicate partition coefficients to 20 GPa and 2800°C: the effects of pressure, temperature, oxygen fugacity, and silicate and metallic melt compositions. *Physics of the Earth and Planetary Interiors* **100**, 115–134.

Robie, R. A., Hemingway, B. S. & Fisher, J. R. (1978). Thermodynamic properties of minerals and related substances at 298·15 K and 1bar (10^5 Pascals) pressure and at higher temperatures. *US Geological Survey Bulletin* **1452.**

Roedder, E. (1983). Geobarometry of ultramafic xenoliths from Loihi Seamount, Hawaii, on the basis of CO_2 inclusions in olivine. *Earth and Planetary Science Letters* **66**, 369–379.

Roeder, P. L. (1974). Activity of iron and olivine solubility in basaltic liquids. *Earth and Planetary Science Letters* **23**, 397–410.

Roeder, P. L. & Emslie, R. F. (1970). Olivine–liquid equilibrium. *Contributions to Mineralogy and Petrology* **29**, 275–289.

Roeder, P. L., Thornber, C., Poustovetov, A. & Grant, A. (2003). Morphology and composition of spinel in Pu'u 'O'o lava (1996–1998), Kilauea volcano, Hawaii. *Journal of Volcanology and Geothermal Research* **123**, 245–265.

Sack, R. O., Carmichael, I. S. E., Rivers, M. & Ghiorso, M. S. (1980). Ferric–ferrous equilibria in natural silicate liquids at 1bar. *Contributions to Mineralogy and Petrology* **75**, 369–376.

Sack, R. O., Walker, D. & Carmichael, I. S. E. (1987). Experimental petrology of alkalic lavas: constraints on cotectics of multiple saturation in natural basic liquids. *Contributions to Mineralogy and Petrology* **96**, 1–23.

Seaman, C., Sherman, S. B., Garcia, M. O., Baker, M. B., Balta, B. & Stolper, E. (2004). Volatiles in glasses from the HSDP2 drill core. *Geochemistry, Geophysics, Geosystems* **5**, Q09G16, doi:10.1029/2003GC000596.

Smith, P. M. & Asimow, P. D. (2005). Adiabat_1ph: A new public front-end to the MELTS, pMELTS, and pHMELTS models. *Geochemistry, Geophysics, Geosystems* **6**, Q02004, doi:10.1029/2004GC000816.

Snyder, D. A. & Carmichael, I. S. E. (1992). Olivine–liquid equilibria and the chemical activities of FeO, NiO, Fe_2O_3, and MgO in natural basic melts. *Geochimica et Cosmochimica Acta* **56**, 303–318.

Sobolev, A. V. & Nikogosian, I. K. (1994). Petrology of long-lived mantle plume magmatism: Hawaii, Pacific, and Reunion Island, Indian Ocean. *Petrology* **2**, 111–144.

Sobolev, A. V., Hofmann, A. W., Kuzmin, D. V. *et al.* (2007). The amount of recycled crust in sources of mantle-derived melts. *Science* **316**, 412–417.

Stolper, E., Sherman, S., Garcia, M., Baker, M. & Seaman, C. (2004). Glass in the submarine section of the HSDP2 drill core, Hilo, Hawaii. *Geochemistry, Geophysics, Geosystems* **5**, Q07G15, doi:10.1029/2003GC000553.

Sugawara, T. (2000). Empirical relationships between temperature, pressure, and MgO content in olivine and pyroxene saturated liquid. *Journal of Geophysical Research* **105**, 8457–8472.

Thornber, C. R., Heliker, C., Sherrod, D. R., Kauahikaua, J. P., Miklus, A., Okubo, P. G., Trusdell, F. A., Budahn, J. R., Ridley, W. I. & Meeker, G. P. (2003). Kilauea East Rift Zone magmatism: an episode 54 perspective. *Journal of Petrology* **44**, 1525–1559.

Thy, P. (1995). Low-pressure experimental constraints on the evolution of komatiites. *Journal of Petrology* **36**, 1529–1548.

Thy, P., Lesher, C. E., Nielsen, T. F. D. & Brooks, C. K. (2006). Experimental constraints on the Skaergaard liquid line of descent. *Lithos* **92**, 154–180.

Toplis, M. J. (2005). The thermodynamics of iron and magnesium partitioning between olivine and liquid: criteria for assessing and predicting equilibrium in natural and experimental systems. *Contributions to Mineralogy and Petrology* **149**, 22–39.

Tsuchiyama, A., Nagahara, H. & Kushiro, I. (1981). Volatilization of sodium from silicate melt spheres and its application to the formation of chondrules. *Geochimica et Cosmochimica Acta* **45**, 1357–1367.

Wagner, T. P. & Grove, T. L. (1998). Melt/harzburgite reaction in the petrogenesis of tholeiitic magma from Kilauea volcano, Hawaii. *Contributions to Mineralogy and Petrology* **131**, 1–12.

Walter, M. J. (1998). Melting of garnet peridotite and the origin of komatiite and depleted lithosphere. *Journal of Petrology* **39**, 29–60.

Wilson, A. D. (1960). The micro-determination of ferrous iron in silicate-minerals by a volumetric and a colorimetric method. *Analyst* **85**, 823–827.

Wright, T. L. (1984). Origin of Hawaiian tholeiite: a metasomatic model. *Journal of Geophysical Research* **89**, 3233–3252.

Xirouchakis, D., Hirschmann, M. M. & Simpson, J. A. (2001). The effect of titanium on the silica content and on mineral–liquid partitioning of mantle-equilibrated melts. *Geochimica et Cosmochimica Acta* **65**, 2201–2217.

Yokoyama, T. & Nakamura, E. (2002). Precise determination of ferrous iron in silicate rocks. *Geochimica et Cosmochimica Acta* **66**, 1085–1093.

Yu, Y., Hewins, R. H., Alexander, C. M. O'D. & Wang, J. (2003). Experimental study of evaporation and isotopic mass fractionation of potassium in silicate melts. *Geochimica et Cosmochimica Acta* **67**, 773–786.